Journal of Thermal Stresses, 23:797–831, 2000

0149-5739/00 $12.00 + .00

AN ASSESSMENT OF MIXED AND CLASSICAL THEORIES FOR THE THERMAL STRESS ANALYSIS OF ORTHOTROPIC MULTILAYERED PLATES

Erasmo Carrera
Department of Aeronautics and Aerospace Engineering
Politecnico di Torino
Italy

This article compares theories formulated on the basis of the classical Principle of Virtual Displacements (PVD) to mixed theories formulated on the basis of the Reissner Mixed Variational Theorem (RMVT) to evaluate the thermal response of orthotropic laminated plates. So-called layer-wise (LW) and equivalent-single-layer (ESL) modelings have been developed for both classical and mixed approaches (each layer is considered as a single plate for LW analysis, while the unknown variables are independent of the number of the constitutive layers for the ESL cases). Linear up-to fourth-order displacement and stress field cases have been implemented to derive thermomechanical governing equations, consistent with the used variational statements. All the theories have been presented in a unified manner by referring to findings recently presented by the author. The numerical investigation has been restricted to a simply supported plate loaded by harmonic distribution of in-plane temperature fields. Constant and linear through-the-thickness temperature distributions have been considered for which exact three-dimensional solutions are available. The results of in-plane and out-of-plane displacement and stress components are given in the form of tables and diagrams. The superiority of the mixed approach to the PVD formulation has been confirmed. Higher order, layer-wise expansions for the unknown variables are required for an accurate description of the thermomechanical response of thick multilayered plates. It has been found that the thickness temperature distributions $T(z)$ have a significant influence on the accuracy of the considered theories.

Stress fields related to temperature variations often represent a contributing factor and, in some cases, are the main cause of the failure of structures. Thin-walled members of reactor vessels, turbines, as well as the structures of future supersonic and hypersonic vehicles, such as that of high-speed civil transport and advanced tactical fighters, are particularly susceptible to failure resulting from excessive stress levels induced by thermal or combined thermomechanical loadings. Furthermore, thermal deformations play a fundamental role in multilayered thin-film regions, comprising optical mirrors. Due to their detrimental implications, the effects of both

Received 17 September 1999; accepted 3 January 2000.
Address correspondence to Dr. Erasmo Carrera, Department of Aeronautics and Aerospace Engineering, Politecnico di Torino, Corso Duca degli Abruzzi, 24, 10129 Torino, Italy. E-mail: carrera@polito.it

high-temperature and mechanical loadings have to be considered in the earliest stages of the design process of such structures [1]. Nevertheless, large portions of the aforementioned structures are made up of multilayered plate and shell constructions such as traditional sandwich panels, panels made of anisotropic composite materials or layered isotropic structures used as thermal protection.

An accurate description of local stress fields in the layers becomes mandatory to prevent thermally loaded structures' failure mechanisms. Early [2, 3] and recent [4–6] exact three-dimensional solutions have shown that appropriate structural modelings are required to describe what was summarized by Carrera [7] with the acronym C_z^0-requirements: the so-called *zig-zag* form of displacement fields and the *interlaminar continuity* for transverse stress fields are C^0-continuous functions in the plate thickness direction z.

Several reviews are available on this topic. Among these mention can be made of the excellent surveys by Tauchert [8], Noor and Burton [9], Argyris and Tenek [10] and the recent book by Reddy [11]. Interested readers can refer to these for a complete overview and literature. A few contributions that have been considered useful by the author and are related to the bending of anisotropic plates are discussed in the following text.

The first reported study on thermal bending of anisotropic thin plates was reported by Pell [12]. Thereafter, Stavsky [13] developed a thermoelastic theory for heterogeneous anisotropic plates. Wu and Tauchert [14, 15] considered simply supported orthotropic plates. Thick-plate theory, which accounts for transverse shear deformation effects, was then considered by Ambartsumian [16], Rath and Das [17], and Tholkachev and Shpektorov [18]. Whitney's [19] isothermal theory was extended to thermal problems by Reddy et al. [20, 21]. Attempts to partially introduce the C_z^0-requirements have been made both in the field of the *equivalent single-layer model* (ESLM) and *layer-wise models* (LWM). According to Reddy [11], in comparison with LWM analyses, ESLMs preserve the independence of the number of the unknowns from the numbers of the layers, permitting advantageous extension to computational mechanics. Refined models that partially account for C_z^0-requirements have been considered by Khorosun [22], Pankratova et al. [23], Cho Striz and Bert [24], Kheider and Reddy [25], and Murakami [4]. In particular, this last article concluded that "in order to predict rapid variation of transverse normal strains, a plate theory with cubic variation of in-plane displacement in each layer, rather than over the entire plate thickness, should be adopted. Otherwise full three-dimensional analyses are recommended." In other words, due to the intrinsic through-the-thickness variation of thermal loadings, a layer-wise description is required to accurately describe the local response of layered plates.

The author [7, 26–34] recently proposed and evaluated mixed LW and ESL plate and shell models based on *Reissner's Mixed Variational Theorem* (RMVT) [35, 36] that are able to fulfill C_z^0-requirements completely. This means that, with respect to the classical formulation based on the *Principle of Virtual Displacement* (PVD), Carrera's theory a priori fulfills the interlaminar equilibrium of the transverse shear stresses and permits their evaluation without requiring any post-processing process such as those used in most of the available analyses or in the predictor-corrector procedures of Noor and Burton [37]. Classical models based on PVD were also devel-

oped for comparison purposes by Carrera. The obtained results showed that appropriate layer-wise modelings can lead to a quasi-three-dimensional description of the static and dynamic response of multilayered plates and shells. Better results were, in general, obtained by implementing the mixed models.

Based on these findings, this article extends the mixed layer-wise models to the thermal static response of anisotropic plates. The thermomechanical governing equations are derived for LW and ESL theories based on both PVD and RMVT. A unified notation developed in the author's previous works is used to handle all the considered theories in a unified manner. Numerical results are given for simply supported orthotropic plates loaded by an in-plane harmonic distribution of temperature for which Navier-type closed-form solutions are given.

Bold letters are used for arrays. Indicial notation, subscripts and superscripts, are used extensively to handle the presented derivations in a concise manner. For the sake of completeness, the article provides some derivations and formulae that were also given in the author's previous articles.

STRAINS AND STRESSES

The geometry and Cartesian coordinate system x, y, z of the multilayered plates made of N_l layers are shown in Figure 1. The lamina are considered homogeneous and to operate in the linear elastic range. Stiffness coefficients of Hooke's law for the anisotropic k-lamina are employed in standard form, which reads $\sigma_i^k = \tilde{C}_{ij}^k \varepsilon_j^k$, where subindices i and j range from 1–6 and stand for the index couples 11, 22, 33, 13, 23, and 12. The material is assumed to be orthotropic, as specified by [38, 11]: $\tilde{C}_{14} = \tilde{C}_{24} = \tilde{C}_{34} = \tilde{C}_{64} = \tilde{C}_{15} = \tilde{C}_{25} = \tilde{C}_{35} = \tilde{C}_{65} = 0$. This implies that σ_{xz}^k and σ_{yz}^k depend only on ε_{xz}^k and ε_{yz}^k. In matrix form,

$$\begin{aligned} \boldsymbol{\sigma}_{\mathrm{pH}}^k &= \tilde{\boldsymbol{C}}_{\mathrm{pp}}^k \boldsymbol{\varepsilon}_{\mathrm{pG}}^k + \tilde{\boldsymbol{C}}_{\mathrm{pn}}^k \boldsymbol{\varepsilon}_{\mathrm{nG}}^k \\ \boldsymbol{\sigma}_{\mathrm{nH}}^k &= \tilde{\boldsymbol{C}}_{\mathrm{np}}^k \boldsymbol{\varepsilon}_{\mathrm{pG}}^k + \tilde{\boldsymbol{C}}_{\mathrm{nn}}^k \boldsymbol{\varepsilon}_{\mathrm{nG}}^k \end{aligned} \tag{1}$$

in which subscripts p, n denote in-plane and out-of-plane (normal) components ($\boldsymbol{\sigma}_{\mathrm{p}}^k = \{\sigma_{xx}^k, \sigma_{yy}^k, \sigma_{xy}^k\}$, $\boldsymbol{\sigma}_{\mathrm{n}}^k = \{\sigma_{xz}^k, \sigma_{yz}^k, \sigma_{zz}^k\}$); H and G indicate values from Hooke's law and from Geometrical Eq. (5) relations, respectively; and the subscript d denotes values related to the standard displacement formulation.

Thermal stresses (subscript T) are induced in the k-layer by thermal strains according to material behavior as follows

$$\begin{aligned} \boldsymbol{\sigma}_{\mathrm{pT}_d}^k &= \tilde{\boldsymbol{C}}_{\mathrm{pp}}^k \boldsymbol{\varepsilon}_{\mathrm{pT}}^k + \tilde{\boldsymbol{C}}_{\mathrm{pn}}^k \boldsymbol{\varepsilon}_{\mathrm{nT}}^k \\ \boldsymbol{\sigma}_{\mathrm{nT}_d}^k &= \tilde{\boldsymbol{C}}_{\mathrm{np}}^k \boldsymbol{\varepsilon}_{\mathrm{pT}}^k + \tilde{\boldsymbol{C}}_{\mathrm{nn}}^k \boldsymbol{\varepsilon}_{\mathrm{nT}}^k \end{aligned} \tag{2}$$

where the strains are related to a given temperature gradient $T^k(x, y, z)$ according to

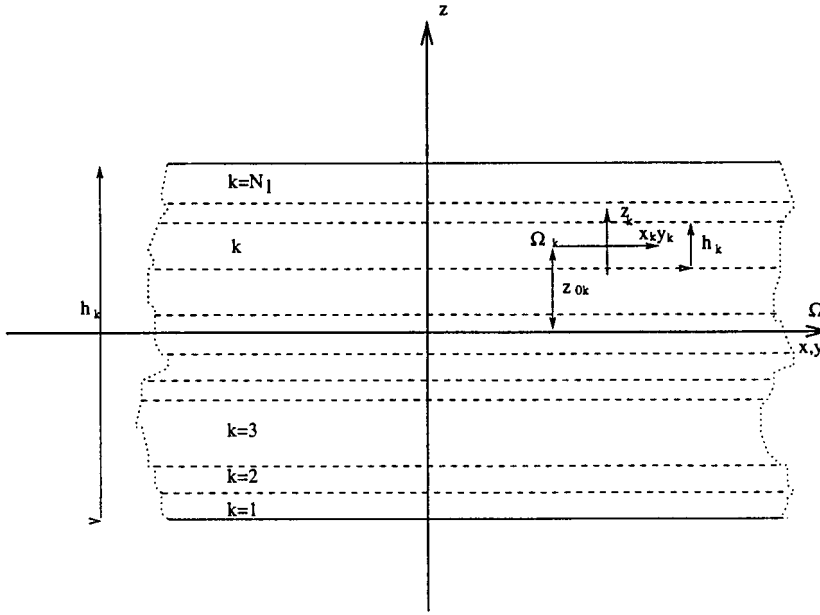

Figure 1. Multilayered plate.

the thermal expansion coefficients α_{ij} of the layer

$$\begin{aligned} \varepsilon^k_{\mathrm{pT}} &= \{\alpha^k_{xx}, \alpha^k_{yy}, \alpha^k_{xy}\}T^k(x,y,z) = \alpha^k_{\mathrm{p}}T^k(x,y,z) \\ \varepsilon^k_{\mathrm{nT}} &= \{\alpha^k_{xz}, \alpha^k_{yz}, \alpha^k_{zz}\}T^k(x,y,z) = \alpha^k_{\mathrm{n}}T^k(x,y,z) \end{aligned} \tag{3}$$

For the adopted mixed solution procedure, the stress-strain relationships are conveniently put in the mixed form

$$\begin{aligned} \sigma^k_{\mathrm{pH}} &= \boldsymbol{C}^k_{\mathrm{pp}}\varepsilon^k_{\mathrm{pG}} + \boldsymbol{C}^k_{\mathrm{pn}}\sigma^k_{\mathrm{nM}} \\ \varepsilon^k_{\mathrm{nH}} &= \boldsymbol{C}^k_{\mathrm{np}}\varepsilon^k_{\mathrm{pG}} + \boldsymbol{C}^k_{\mathrm{nn}}\sigma^k_{\mathrm{nM}} \end{aligned} \tag{4}$$

where both stiffness and compliance coefficients are employed. Subscript M denotes stress from the assumed model Eq. (9). The relations between the arrays of coefficients of the two forms of Hooke's law are easily found

$$\begin{aligned} \boldsymbol{C}^k_{\mathrm{pp}} &= \tilde{\boldsymbol{C}}^k_{\mathrm{pp}} - \tilde{\boldsymbol{C}}^k_{\mathrm{pn}}(\tilde{\boldsymbol{C}}^k_{\mathrm{nn}})^{-1}\tilde{\boldsymbol{C}}^k_{\mathrm{np}} \qquad & \boldsymbol{C}^k_{\mathrm{pn}} &= \tilde{\boldsymbol{C}}^k_{\mathrm{pn}}(\tilde{\boldsymbol{C}}^k_{\mathrm{nn}})^{-1} \\ \boldsymbol{C}^k_{\mathrm{np}} &= -(\tilde{\boldsymbol{C}}^k_{\mathrm{nn}})^{-1}\tilde{\boldsymbol{C}}^k_{\mathrm{np}} & \boldsymbol{C}^k_{\mathrm{nn}} &= (\tilde{\boldsymbol{C}}^k_{\mathrm{nn}})^{-1} \end{aligned}$$

where superscripts -1 indicate the inverse of a square array.

Thermal stresses and strains related to the mixed procedure are computed by using Eqs. (2) and (3). The strain components $\varepsilon_{\mathrm{p}}^{k} = \{\varepsilon_{xx}^{k}, \varepsilon_{yy}^{k}, \varepsilon_{xy}^{k}\}$, $\varepsilon_{\mathrm{n}}^{k} = \{\varepsilon_{xz}^{k}, \varepsilon_{yz}^{k}, \varepsilon_{zz}^{k}\}$ are linearly related to the displacements $\boldsymbol{u}^{k} = \{u_{x}^{k}, u_{y}^{k}, u_{z}^{k}\}$ according to the geometrical relations

$$\varepsilon_{\mathrm{pG}}^{k} = \boldsymbol{D}_{\mathrm{p}}\boldsymbol{u}^{k} \qquad \varepsilon_{\mathrm{nG}}^{k} = \boldsymbol{D}_{\mathrm{n}}\boldsymbol{u}^{k} \tag{5}$$

where $\boldsymbol{D}_{\mathrm{p}}$ and $\boldsymbol{D}_{\mathrm{n}}$ denote in-plane and out-of-plane differential operators, respectively. Explicit forms of the introduced arrays are provided in the appendix.

DISPLACEMENT AND TRANSVERSE STRESS MODELS

A displacement field in the plate thickness direction is usually assumed in the framework of a classical formulation based on PVD, while the RMVT [35, 36] permits one to assume two independent fields for the displacement and transverse stress fields. Both assumptions have been discussed by the author in the previously mentioned article. For the sake of completeness, a short description of the meanings of several variables written in unified notation follows. Displacement and stress fields for ESLMs and LWMs are considered.

Single-layer Theories or ESLM

First, the theory in which the number of displacement variables is taken independent of the number of the constitutive layer N_l is considered.

Displacement field. By referring to the Murakami idea [39], the zig-zag form of the displacement fields can be reproduced in an equivalent single-layer description. Such an idea adds a zig-zag term into a classical Taylor-type expansion in the thickness plate direction of the unknown displacements in the neighborhood of the reference plate surface Ω (Figure 2*a*). The displacement model in [39] is herein written in the following generalized form,

$$\boldsymbol{u} = \boldsymbol{u}_0 + (-1)^{k}\zeta_k\,\boldsymbol{u}_z + z^{r}\,\boldsymbol{u}_r \qquad r = 1, 2, \ldots, N \tag{6}$$

where N is a free parameter of the model, the repeated indexes r are summed over their ranges, subscript 0 denotes values related to the plate reference surface Ω, and subscript Z refers to the introduced zig-zag term. Higher order distributions in the z-direction are introduced by the r-polynomials. In order to give a unified form for the assumed models, the same notation that will be employed in the layer-wise description should be conveniently used in Eqs. (6), which is therefore rewritten as

$$\boldsymbol{u} = F_t\,\boldsymbol{u}_t + F_b\,\boldsymbol{u}_b + F_r\,\boldsymbol{u}_r = F_\tau\,\boldsymbol{u}_\tau \qquad \tau = t, b, r \quad r = 1, 2, \ldots, N \tag{7}$$

where subscript b denotes values related to the plate reference surface Ω ($\boldsymbol{u}_b = \boldsymbol{u}_0$) while subscript t refers to the introduced zig-zag term ($\boldsymbol{u}_t = \boldsymbol{u}_Z$). The functions

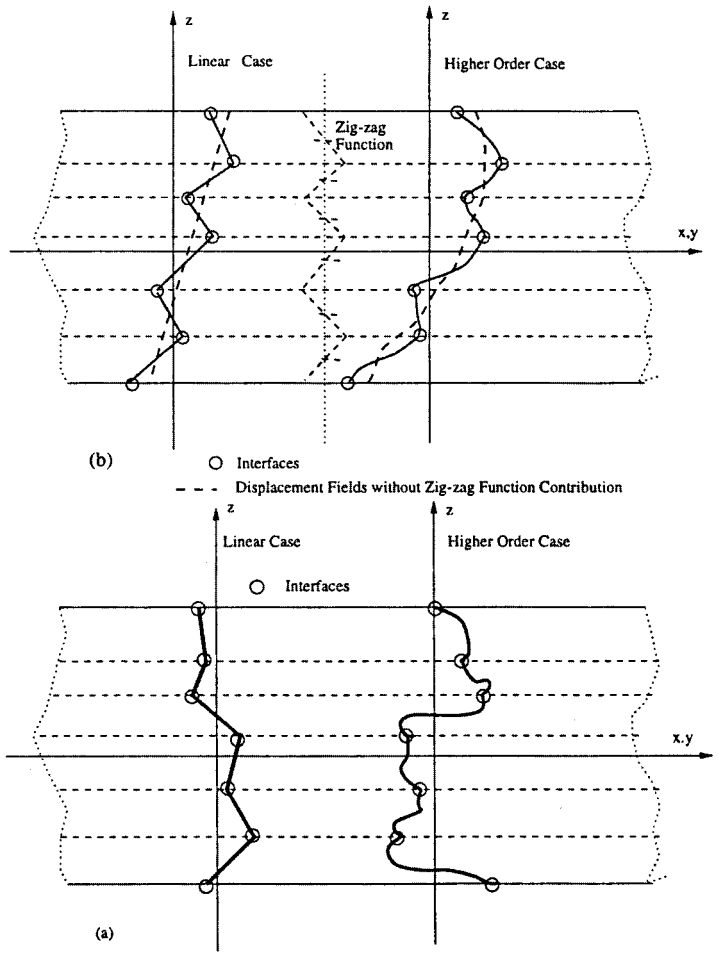

Figure 2. Displacement and stress fields assumed for the employed models.

F_τ assume the explicit form

$$F_b = 1 \qquad F_t = (-1)^k \zeta_k \qquad F_r = z^r \quad \text{for} \quad r = 1, 2, \ldots, N \tag{8}$$

Notice that F_t assumes the values ± 1 corresponding to the bottom and the top interfaces of the k-layer (Figure 2*a*). The term $\boldsymbol{u}_t$ is considered constant in Eqs. (7). This fact constitutes the fundamental limitation of the considered single-layer models.

Transverse stress field. RMVT requires the assumptions of an independent transverse stress field. The thickness expansion used for displacement variables in Eqs. (7) is not suitable for transverse stresses; for instance, homogeneous top-bottom plate surface conditions could not be imposed. Therefore, transverse

stresses are herein described by means of the following layer-wise description [7, 27, 39]

$$\sigma^k_{\mathrm{nM}} = F_{\mathrm{t}}\sigma^t_{\mathrm{nt}} + F_{\mathrm{b}}\sigma^k_{\mathrm{nb}} + F_r\sigma^k_{\mathrm{n}r} = F_\tau\sigma^k_{\mathrm{n}\tau} \qquad \tau = \mathrm{t}, \mathrm{b}, r, \quad r = 2, 3, \ldots, N, \quad k = 1, 2, \ldots, N_l \tag{9}$$

In contrast to what appears in Eqs. (7), it is now intended that the subscripts t and b denote values related to the layer top and bottom surfaces, respectively. They consist of the linear part of the expansion. The thickness functions $F_\tau(\zeta_k)$ have been defined by

$$F_{\mathrm{t}} = \frac{P_0 + P_1}{2} \qquad F_{\mathrm{b}} = \frac{P_0 - P_1}{2} \qquad F_r = P_r - P_{r-2} \ \text{ for } \ r = 2, 3, \ldots, N \tag{10}$$

in which $P_j = P_j(\zeta_k)$ is the Legendre polynomial of the j-order defined in the ζ_k-domain: $-1 \le \zeta_k \le 1$. A fourth-order case will be used in the numerical investigations; related polynomials are

$$P_0 = 1 \qquad P_1 = \zeta_k \qquad P_2 = (3\zeta_k^2 - 1)/2$$
$$P_3 = \frac{5\zeta_k^3}{2} - \frac{3\zeta_k}{2} \qquad P_4 = \frac{35\zeta_k^2}{8} - \frac{15\zeta_k^2}{4} + \frac{3}{8}$$

The chosen functions have the properties

$$\zeta_k = \begin{cases} 1: & F_{\mathrm{t}} = 1, \quad F_{\mathrm{b}} = 0, \quad F_r = 0 \\ -1: & F_{\mathrm{t}} = 0, \quad F_{\mathrm{b}} = 1, \quad F_r = 0 \end{cases} \tag{11}$$

The top and bottom values have been used as unknown variables. The interlaminar transverse shear and normal stress continuity can therefore be easily linked

$$\sigma^k_{\mathrm{nt}} = \sigma^{(k+1)}_{\mathrm{nb}} \qquad k = 1, \ N_l - 1 \tag{12}$$

In those cases in which top/bottom-shell stress values are prescribed (zero or imposed values), the following additional equilibrium conditions must be accounted for

$$\sigma^1_{\mathrm{nb}} = \bar{\sigma}_{\mathrm{nb}} \qquad \sigma^{N_l}_{\mathrm{nt}} = \bar{\sigma}_{\mathrm{nt}} \tag{13}$$

where the overbar denotes imposed values in correspondence to the plate boundary surfaces. Examples of linear and higher order fields are plotted in Figure 2*b*.

Note that ESLMs lead to a set of constitutive equations, the number of which is N_l-dependent (see next developments). From this point of view, calling them "single-layer" does not seem very appropriate. Their use, however, can be justified by the fact that the stress variables can be eliminated in the numerical solution process.

Layer-wise Models

Layer-wise or multi-layer modelings were mainly proposed to remove ESLM-type assumptions made for the zig-zag amplitude u_Z. In fact, the last three decades of literature has shown that such an amplitude is layer-dependent. Layer-wise fields are assumed for both displacement and stress variables as in Eqs. (9),

$$\begin{aligned} \boldsymbol{u}^k &= F_{\mathrm{t}}\boldsymbol{u}^k_{\mathrm{t}} + F_{\mathrm{b}}\boldsymbol{u}^k_{\mathrm{b}} + F_r\boldsymbol{u}^k_r = F_\tau\boldsymbol{u}^k_\tau \qquad & \tau = \mathrm{t}, \mathrm{b}, r \\ & & r = 2, 3, \ldots, N \\ \sigma^k_{\mathrm{nM}} &= F_{\mathrm{t}}\sigma^k_{\mathrm{nt}} + F_{\mathrm{b}}\sigma^k_{\mathrm{nb}} + F_r\sigma^k_{\mathrm{n}r} = F_\tau\sigma^k_{\mathrm{n}\tau} \qquad & k = 1, 2, \ldots, N_l \end{aligned} \tag{14}$$

In addition to Eqs. (12), the compatibility of the displacement requires that

$$\boldsymbol{u}^k_{\mathrm{t}} = \boldsymbol{u}^{(k+1)}_{\mathrm{b}} \qquad k = 1, N_l - 1 \tag{15}$$

Equations (14) refer to the same order of expansion for the three components of $\boldsymbol{u}^k$ and σ_n. In order to conform to well-known results in the literature (see, for example, the author's discussion reported in [7, 28]), different polynomial orders should be used in developments that are presented in the subsequent sections. Trace operators that would lead to a shortening of the resulting arrays could be introduced for this purpose. For the sake of brevity, the results related to these aspects have not been discussed. These could be more conveniently reported in future works.

Summary with Acronyms and the Considered Theories

Depending on the type of formulation (PVD or RMVT), variables description (LW or ESLM), and order of the used expansion, for example, a number of two-dimensional theories can be constructed on the basis of the two-dimensional modelings described in this section. In order to identify these theories concisely, acronyms will be extensively used in the numerical parts. Figure 3 shows how such acronyms have been built. Examples of displacement and stress fields related to a few particular-case theories are plotted in Figure 4. Some comments to these plots follow. Transverse stress and displacement z-fields are the same for the LM1 (layer-wise mixed linear) and LM3 (layer-wise mixed cubic) descriptions, while only displacement assumptions are made for LD1 (layer-wise displacement linear) and LD3 (layer-wise displacement cubic) cases. The parabolic transverse stress field in each layer is associated with a linear zig-zag displacement field for the EMZC1 case (equivalent-single-layer mixed zig-zag interlaminar-continuity linear), and the fourth-order transverse stress field in each layer is associated with the cubic zig-zag displacement field for the EMZC3 case (equivalent-single-layer mixed zig-zag interlaminar-continuity cubic). Note the geometrical meaning of the use of the zig-zag function due to Murakami [39]: a linear through-the-thickness function of constant amplitude and opposite sign for two adjacent layers is added to a Taylor-type linear (or cubic for EMZC3) formulation in order to force discontinuous derivatives in z for the displacement components.

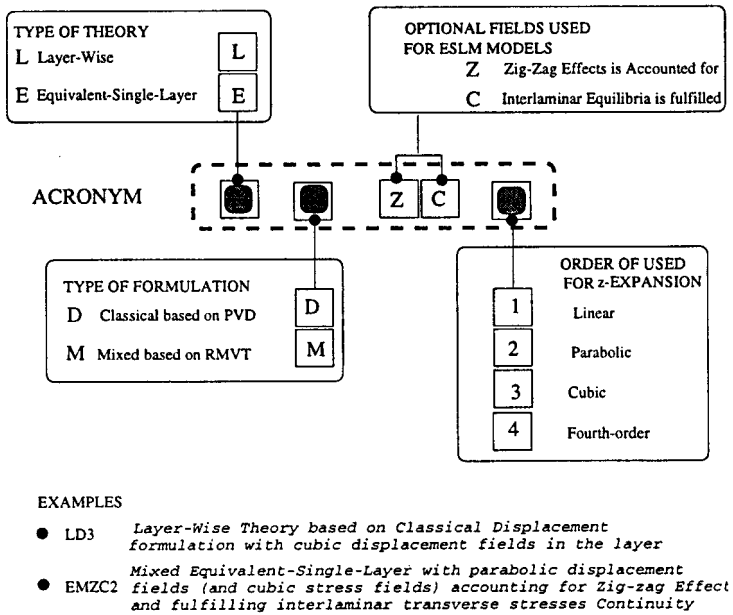

Figure 3. Meanings of the introduced acronyms.

TEMPERATURE DISTRIBUTION WITH PLATE-THICKNESS

For our convenience and without losing generality, the given temperature field along the layer thickness can be expressed through the Legendre polynomials as the stress and displacement field. Therefore, the temperature rise in the layer is assumed

$$T^k(x, y, z) = F_t T_t^k + F_b T_b^k + F_2 T_2^k = F_\tau T_\tau^k. \tag{16}$$

Here T^k are the values given with respect to the environmental temperature T_e

$$T_\tau^k = \bar{T}_\tau^k - T_e$$

where $\bar{T}_\tau^k$ are the effective temperatures in the plate.

Note that the distribution of temperature with thickness for a given set of thermal boundary conditions at the lateral top and bottom surfaces of the plates can be obtained by solving the heat conduction equation (see, e.g., [5]). For the case of laminates, such a solution has shown that the thickness temperature distribution $T(z)$ is of C_z^0-type, so it could be handled easily by Eq. (16). However, only a simple linear antisymmetric (with respect to z) variation is considered here in the numerical investigation, as this would apply to bending (without stretching) of a symmetric laminate and would be adequate to bring out important nonclassical influences such as C_z^0-requirements, transverse shear deformation, and thickness strains.

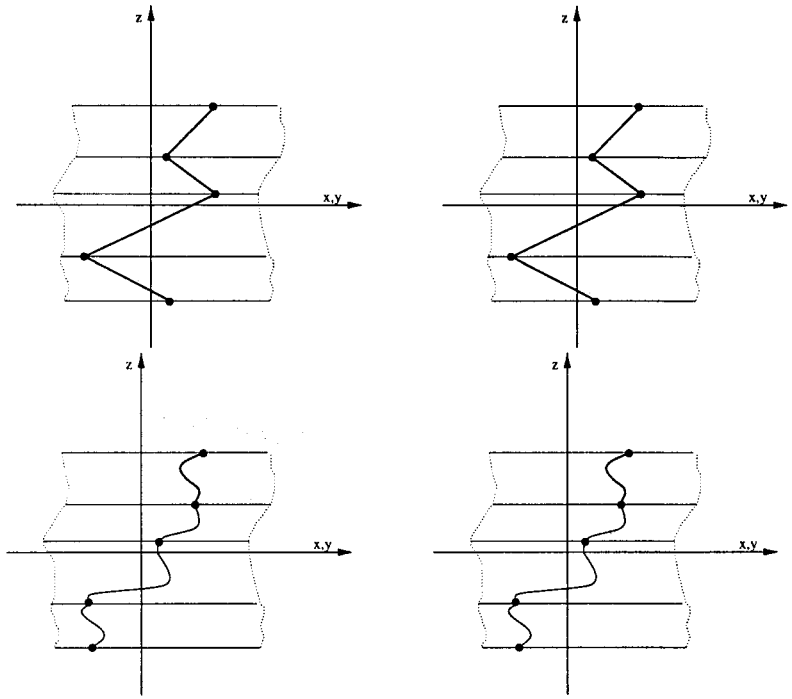

LM1 (upper part) and LM3 (lower part) displacement (left) and stress (right) fields.

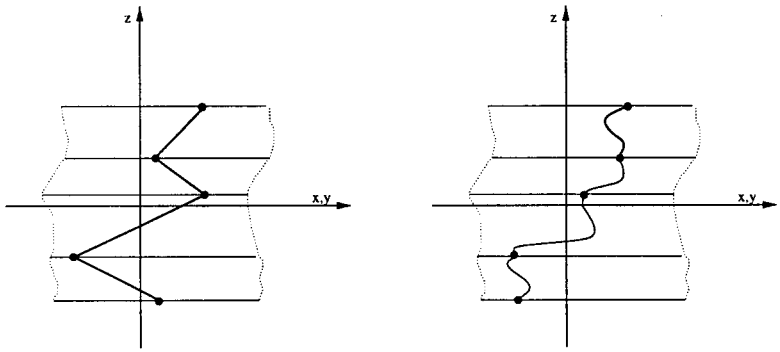

LD1 (left) and LD3 (right) displacement fields.

Figure 4. Examples of assumed fields in the thickness plate direction in a four-layered plate.

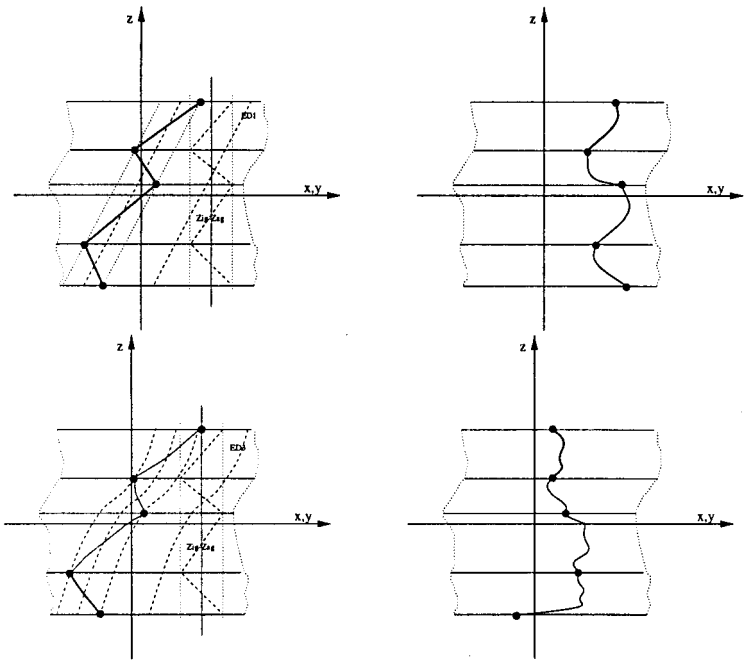

EMZC1 (upper part) and EMZC3 (lower part) displacement (left) and stress (right) fields.

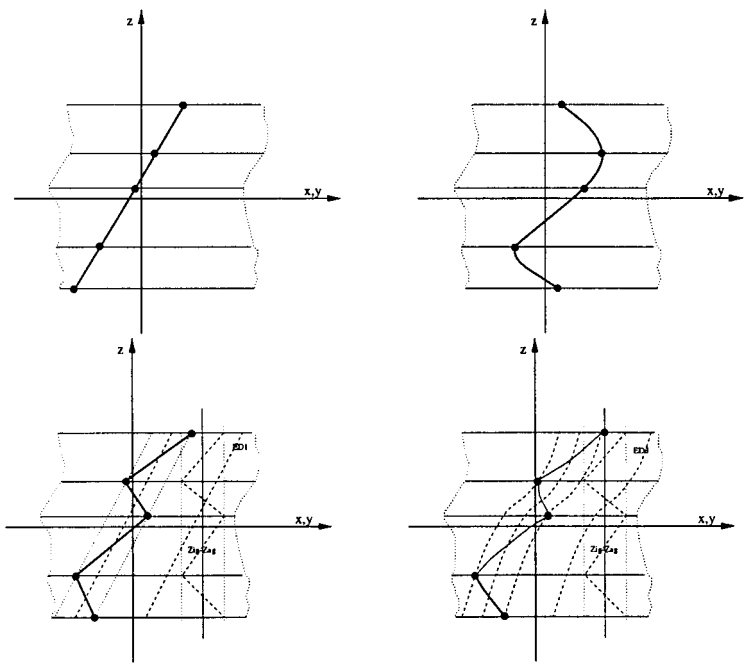

ED1, ED3 (upper part) and EDZ1 and EDZ3 (lower part) displacement fields.

Figure 4. *cont.*.

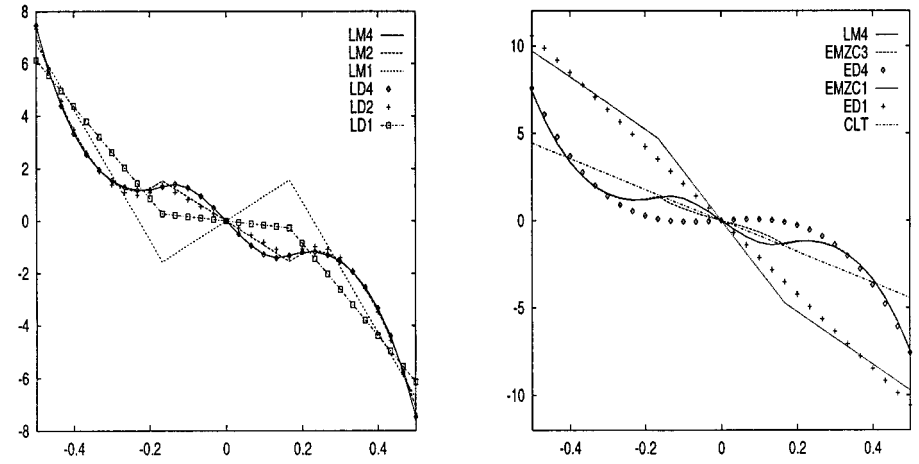

Figure 4. *cont.*. $\bar{U}_z$ vs z: LW (left) and ESLM (right) thick plate $a/h = 4$. Cylindrical bending problem.

GOVERNING EQUATIONS FOR THE k-LAYER

Displacement Formulation Based on PVD

The classical displacement approach is formulated in terms of $\boldsymbol{u}^k$ via the principle of virtual displacements. In the static case and in the presence of thermal stresses, this principle states

$$\sum_{k=1}^{N_l} \int_{\Omega^k} \int_{A_k} \left(\delta \varepsilon_{\mathrm{pG}}^{k\mathrm{T}} \left(\sigma_{\mathrm{pH}_d}^k - \sigma_{\mathrm{pT}}^k \right) + \delta \varepsilon_{\mathrm{nG}}^{k\mathrm{T}} \left(\sigma_{\mathrm{nH}_d}^k - \sigma_{\mathrm{nT}}^k \right) \right) d\Omega^k \, dz = \delta L^{\mathrm{e}} \qquad (17)$$

where δ is the variational symbol; subscript T denotes transposition of arrays; A_k and V denote the layer-thickness domain and volume, respectively; and Ω^k is the layer middle surface bounded by Γ^k (Γ_{g}^k, Γ_{m}^k denotes those parts of Γ^k on which the geometrical and mechanical boundary conditions are prescribed, respectively). The variation of the internal work has been split into in-plane and out-of-plane parts and involves stress from Hooke's Law and strain from geometrical relations. δL_{e} is the virtual variation of the work made by the external layer-forces $\boldsymbol{p}^k = \{p_x^k, p_y^k, p_z^k\}$.

In order to handle the next developments in a concise manner, it is convenient to do as follows.

1. The displacement models Eqs. (7) and (9) are substituted into the strains

$$\varepsilon_{\mathrm{pG}}^k = \boldsymbol{D}_{\mathrm{p}} F_\tau \boldsymbol{u}_\tau^k \qquad \varepsilon_{\mathrm{nG}}^k = (\boldsymbol{D}_{\mathrm{n}\Omega} + \boldsymbol{D}_{\mathrm{n}z}) \boldsymbol{u}^k = \boldsymbol{D}_{\mathrm{n}\Omega} F_\tau \boldsymbol{u}_\tau^k + F_{\tau_z} \boldsymbol{u}_\tau^k \qquad (18)$$

where the subscript z denotes differentiation with respect to z.

2. The following stress-layer resultants are defined as

$$\left(\mathcal{R}^{k\tau}_{\mathrm{pH}_d}, \mathcal{R}^{k\tau}_{\mathrm{nH}_d}, \mathcal{R}^{k\tau_z}_{\mathrm{nH}_d}\right) = \int_{A_k} \left(F_\tau \sigma^k_{\mathrm{pH}_d}, F_\tau \sigma^k_{\mathrm{nH}_d}, F_{\tau_z} \sigma^k_{\mathrm{nH}_d}\right) dz$$
$$\left(\mathcal{R}^{k\tau}_{\mathrm{pT}}, \mathcal{R}^{k\tau}_{\mathrm{nT}}, \mathcal{R}^{k\tau_z}_{\mathrm{nT}}\right) = \int_{A_k} \left(F_\tau \sigma^k_{\mathrm{pT}}, F_\tau \sigma^k_{\mathrm{nT}}, F_\tau \sigma^k_{\mathrm{nT}}\right) dz \tag{19}$$

3. The following array formula for the integration by parts is introduced

$$\int_{\Omega^k} (\boldsymbol{D}_\Omega \phi)^{\mathrm{T}}\, \phi \, d\Omega^k = -\int_{\Omega^k} \varphi^{\mathrm{T}} \boldsymbol{D}^{\mathrm{T}}_\Omega \phi \, d\Omega^k + \int_{\Gamma^k} \varphi^{\mathrm{T}} \boldsymbol{I}^{\mathrm{T}}_\Omega \phi \, d\Gamma^k$$

For the sake of simplicity, it is intended that the boundary Γ^k is parallel to the direction x, y; φ and ϕ are two generic columns of displacements or stresses; $\boldsymbol{D}_\Omega$ denotes a generic array including only first-order partial differential operators with respect to the in-plane coordinates x, y. The algebraic array $\boldsymbol{I}^{\mathrm{T}}_\Omega$ is built as follows: the unit number 1 is set in correspondence to those elements of $\boldsymbol{D}_\Omega$, which are different from zero (see Appendix A).

Based on this, Eq. (17) takes on the form

$$\sum_{k=1}^{N_l} \left(\int_{\Omega^k} \delta \boldsymbol{u}^{k\mathrm{T}}_\tau \left(-\boldsymbol{D}^{\mathrm{T}}_{\mathrm{p}} \left(\mathcal{R}^{k\tau}_{\mathrm{pH}_d} - \mathcal{R}^{k\tau}_{\mathrm{pT}} \right) + \mathcal{R}^{k\tau_z}_{\mathrm{nH}_d} + \mathcal{R}^{k\tau_z}_{\mathrm{nT}} - \boldsymbol{D}^{\mathrm{T}}_{\mathrm{n}\Omega} \left(\mathcal{R}^{k\tau}_{\mathrm{nH}_d} - \mathcal{R}^{k\tau}_{\mathrm{nT}} \right) \right) d\Omega^k \right.$$
$$\left. + \int_{\Gamma^k} \delta \boldsymbol{u}^{k\mathrm{T}}_\tau \left(\boldsymbol{I}^{\mathrm{T}}_{\mathrm{p}} \left(\mathcal{R}^{k\tau}_{\mathrm{pH}_d} - \mathcal{R}^{k\tau}_{\mathrm{pT}} \right) + \boldsymbol{I}^{\mathrm{T}}_{\mathrm{n}\Omega} \left(\mathcal{R}^{k\tau}_{\mathrm{nH}_d} - \mathcal{R}^{k\tau}_{\mathrm{nT}} \right) \right) d\Gamma^k \right)$$
$$= \sum_{k=1}^{N_l} \int_{\Omega^k} \delta \boldsymbol{u}^{k\mathrm{T}}_\tau \boldsymbol{p}^k_\tau \, d\Omega^k$$

where $\boldsymbol{p}^k_\tau = \{p^k_{x\tau}, p^k_{y\tau}, p^k_{z\tau}\}$ are the variationally consistent load vector due to $\boldsymbol{p}^k$. By imposing the definition of virtual variations for the unknown displacements, the differential system of governing equations and related boundary conditions are derived in terms of the introduced stress resultants. For the k-layer, the equilibrium equations on Ω^k are

$$\delta \boldsymbol{u}^k_\tau : \quad -\boldsymbol{D}^{\mathrm{T}}_{\mathrm{p}} \left(\mathcal{R}^{k\tau}_{\mathrm{pH}_d} - \mathcal{R}^{k\tau}_{\mathrm{pT}} \right) + \mathcal{R}^{k\tau_z}_{\mathrm{nH}_d} + \mathcal{R}^{k\tau_z}_{\mathrm{nT}} - \boldsymbol{D}^{\mathrm{T}}_{\mathrm{n}\Omega} \left(\mathcal{R}^{k\tau}_{\mathrm{nH}_d} - \mathcal{R}^{k\tau}_{\mathrm{nT}} \right) = \boldsymbol{p}^k_\tau \tag{21}$$

while the boundary conditions on Γ^k are geometrical on Γ^k_{g}

$$\boldsymbol{u}^k_\tau = \bar{\boldsymbol{u}}^k_\tau \tag{22a}$$

or mechanical on Γ^k_{m}

$$\boldsymbol{I}^{\mathrm{T}}_{\mathrm{p}} \left(\mathcal{R}^{k\tau}_{\mathrm{pH}_d} - \mathcal{R}^{k\tau}_{\mathrm{pT}} \right) + \boldsymbol{I}^{\mathrm{T}}_{\mathrm{n}\Omega} \left(\mathcal{R}^{k\tau}_{\mathrm{nH}_d} - \mathcal{R}^{k\tau}_{\mathrm{nT}} \right) = \boldsymbol{I}^{\mathrm{T}}_{\mathrm{p}} \left(\bar{\mathcal{R}}^{k\tau}_{\mathrm{pH}_d} - \bar{\mathcal{R}}^{k\tau}_{\mathrm{pT}} \right) + \boldsymbol{I}^{\mathrm{T}}_{\mathrm{n}\Omega} \left(\bar{\mathcal{R}}^{k\tau}_{\mathrm{nH}_d} - \bar{\mathcal{R}}^{k\tau}_{\mathrm{nT}} \right) \tag{22b}$$

The overbar denotes imposed values at the boundary. The complete set of equations for the N_l-layers could be written simply by expanding over their ranges the introduced subscripts and superscripts.

In order to express the governing equations in terms of the displacement variables, the stress resultants of Eq. (19) are written in terms of unknown variables u^k by substituting Eqs. (4), (7), (9), and (18) as follows. First, resultants of mechanical stresses are considered

$$\begin{aligned}
\boldsymbol{\mathcal{R}}^{k\tau}_{\mathrm{pH}_d} &= \tilde{\boldsymbol{Z}}^{k\tau s}_{\mathrm{pp}} \boldsymbol{D}_{\mathrm{p}} \boldsymbol{u}^k_s + \tilde{\boldsymbol{Z}}^{k\tau s}_{\mathrm{pn}} \boldsymbol{D}_{\mathrm{n}\Omega} \boldsymbol{u}^k_s + \tilde{\boldsymbol{Z}}^{k\tau s_z}_{\mathrm{pn}} \boldsymbol{D}_{\mathrm{n}\Omega} \boldsymbol{u}^k_s \\
\boldsymbol{\mathcal{R}}^{k\tau}_{\mathrm{nH}_d} &= \tilde{\boldsymbol{Z}}^{k\tau s}_{\mathrm{np}} \boldsymbol{D}_{\mathrm{p}} \boldsymbol{u}^k_s + \tilde{\boldsymbol{Z}}^{k\tau s}_{\mathrm{nn}} \boldsymbol{D}_{\mathrm{n}\Omega} \boldsymbol{u}^k_s + \tilde{\boldsymbol{Z}}^{k\tau s_z}_{\mathrm{nn}} \boldsymbol{u}^k_s \\
\boldsymbol{\mathcal{R}}^{k\tau}_{\mathrm{nH}_d} &= \tilde{\boldsymbol{Z}}^{k\tau_z s}_{\mathrm{np}} \boldsymbol{D}_{\mathrm{p}} \boldsymbol{u}^k_s + \tilde{\boldsymbol{Z}}^{k\tau_z s}_{\mathrm{nn}} \boldsymbol{D}_{\mathrm{n}\Omega} \boldsymbol{u}^k_s + \tilde{\boldsymbol{Z}}^{k\tau_z s_z}_{\mathrm{nn}} \boldsymbol{u}^k_s
\end{aligned} \tag{23}$$

The subscript/superscript $s = \mathrm{t}, \mathrm{b}, 2$ and the following layer-stiffnesses and integrals have been introduced

$$\begin{aligned}
\left(\tilde{\boldsymbol{Z}}^{k\tau s}_{\mathrm{pp}}, \tilde{\boldsymbol{Z}}^{k\tau s}_{\mathrm{pn}}, \tilde{\boldsymbol{Z}}^{k\tau s}_{\mathrm{np}}, \tilde{\boldsymbol{Z}}^{k\tau s}_{\mathrm{nn}}\right) &= \left(\tilde{\boldsymbol{C}}^{k}_{\mathrm{pp}}, \tilde{\boldsymbol{C}}^{k}_{\mathrm{pn}}, \tilde{\boldsymbol{C}}^{k}_{\mathrm{np}}, \tilde{\boldsymbol{C}}^{k}_{\mathrm{nn}}\right) E_{\tau s} \\
\left(\tilde{\boldsymbol{Z}}^{k\tau s_z}_{\mathrm{pn}}, \tilde{\boldsymbol{Z}}^{k\tau_z s}_{\mathrm{np}}, \tilde{\boldsymbol{Z}}^{k\tau s_z}_{\mathrm{nn}}, \tilde{\boldsymbol{Z}}^{k\tau_z s}_{\mathrm{nn}}, \tilde{\boldsymbol{Z}}^{k\tau_z s_z}_{\mathrm{nn}}\right) &= \left(\tilde{\boldsymbol{C}}^{k}_{\mathrm{pn}} E_{\tau s_z}, \tilde{\boldsymbol{C}}^{k}_{\mathrm{np}} E_{\tau_z s}, \tilde{\boldsymbol{C}}^{k}_{\mathrm{nn}} E_{\tau_z s}, \tilde{\boldsymbol{C}}^{k}_{\mathrm{nn}} E_{\tau_z s_z}\right) \\
\left(E^k_{\tau s}, E_{\tau_z s}, E_{\tau s_z}, E^k_{\tau_z s_z}\right) &= \int_{A_k} \left(F_\tau F_s, F_{\tau_z} F_s, F_\tau F_{s_z}, F_{\tau_z} F_{s_z}\right) dz
\end{aligned} \tag{24}$$

The resultants of thermal stresses are

$$\begin{aligned}
\boldsymbol{\mathcal{R}}^{k\tau}_{\mathrm{pT}} &= \tilde{\boldsymbol{V}}^{k\tau s}_{\mathrm{pp}} T^k_s + \tilde{\boldsymbol{V}}^{k\tau s}_{\mathrm{pn}} T^k_s \\
\boldsymbol{\mathcal{R}}^{k\tau}_{\mathrm{nT}} &= \tilde{\boldsymbol{V}}^{k\tau s}_{\mathrm{np}} T^k_s + \tilde{\boldsymbol{V}}^{k\tau s}_{\mathrm{nn}} T^k_s \\
\boldsymbol{\mathcal{R}}^{k\tau_z}_{\mathrm{nT}} &= \tilde{\boldsymbol{V}}^{k\tau_z s}_{\mathrm{np}} T^k_s + \tilde{\boldsymbol{V}}^{k\tau_z s}_{\mathrm{nn}} T^k_s
\end{aligned} \tag{25}$$

where

$$\begin{aligned}
\left(\tilde{\boldsymbol{V}}^{k\tau s}_{\mathrm{pp}}, \tilde{\boldsymbol{V}}^{k\tau s}_{\mathrm{pn}}, \tilde{\boldsymbol{V}}^{k\tau s}_{\mathrm{np}}, \tilde{\boldsymbol{V}}^{k\tau s}_{\mathrm{nn}}\right) &= \left(\tilde{\boldsymbol{C}}^{k}_{\mathrm{pp}} \alpha_{\mathrm{p}}, \tilde{\boldsymbol{C}}^{k}_{\mathrm{pn}} \alpha_{\mathrm{n}}, \tilde{\boldsymbol{C}}^{k}_{\mathrm{np}} \alpha_{\mathrm{p}}, \tilde{\boldsymbol{C}}^{k}_{\mathrm{nn}} \alpha_{\mathrm{n}}\right) E_{\tau s} \\
\left(\tilde{\boldsymbol{V}}^{k\tau_z s}_{\mathrm{np}}, \tilde{\boldsymbol{V}}^{k\tau_z s}_{\mathrm{nn}}\right) &= \left(\tilde{\boldsymbol{C}}^{k}_{\mathrm{np}} \alpha_{\mathrm{p}} E_{\tau_z s}, \tilde{\boldsymbol{C}}^{k}_{\mathrm{nn}} \alpha_{\mathrm{n}} E_{\tau_z s}\right)
\end{aligned} \tag{26}$$

The obtained stress resultants in Eq. (23) can be introduced in Eqs. (21), (34), and (35), leading to equilibrium equations expressed in terms of the displacement variables

$$\delta \boldsymbol{u}^k_\tau : \quad \boldsymbol{K}^{k\tau s}_{\mathrm{d}} \boldsymbol{u}^k_s = \boldsymbol{p}^k_\tau + \boldsymbol{T}^k_\tau \tag{27}$$

with the related boundary conditions

$$\boldsymbol{u}^k_\tau = \bar{\boldsymbol{u}}^k_\tau \quad \text{or} \quad \Pi^{k\tau s}_{\mathrm{d}} \boldsymbol{u}^k_s - {}^{\pi}\boldsymbol{T}^k_\tau = \Pi^{k\tau s}_{\mathrm{d}} \bar{\boldsymbol{u}}^k_s - {}^{\pi}\overline{\boldsymbol{T}}^{k\tau} \tag{28}$$

where

$$
\begin{aligned}
\boldsymbol{K}_{\mathrm{d}}^{k\tau s} &= -\boldsymbol{D}_{\mathrm{p}}^{\mathrm{T}}\left(\tilde{\boldsymbol{Z}}_{\mathrm{pp}}^{k\tau s}\boldsymbol{D}_{\mathrm{p}} + \tilde{\boldsymbol{Z}}_{\mathrm{pn}}^{k\tau s}\boldsymbol{D}_{\mathrm{n}\Omega} + \tilde{\boldsymbol{Z}}_{\mathrm{pn}}^{k\tau s_z}\boldsymbol{D}_{\mathrm{n}\Omega}\right) - \boldsymbol{D}_{\mathrm{n}\Omega}^{\mathrm{T}}\left(\tilde{\boldsymbol{Z}}_{\mathrm{np}}^{k\tau s}\boldsymbol{D}_{\mathrm{p}} + \tilde{\boldsymbol{Z}}_{\mathrm{nn}}^{k\tau s}\boldsymbol{D}_{\mathrm{n}\Omega} + \tilde{\boldsymbol{Z}}_{\mathrm{nn}}^{k\tau s_z}\right) \\
&\quad + \tilde{\boldsymbol{Z}}_{\mathrm{np}}^{k\tau_z s}\boldsymbol{D}_{\mathrm{p}} + \tilde{\boldsymbol{Z}}_{\mathrm{nn}}^{k\tau_z s}\boldsymbol{D}_{\mathrm{n}\Omega} + \tilde{\boldsymbol{Z}}_{\mathrm{nn}}^{k\tau_z s_z} \\
\boldsymbol{\Pi}_{\mathrm{d}}^{k\tau s} &= \boldsymbol{I}_{\mathrm{p}}^{\mathrm{T}}\left(\tilde{\boldsymbol{Z}}_{\mathrm{pp}}^{k\tau s}\boldsymbol{D}_{\mathrm{p}} + \tilde{\boldsymbol{Z}}_{\mathrm{pn}}^{k\tau s}\boldsymbol{D}_{\mathrm{n}\Omega} + \tilde{\boldsymbol{Z}}_{\mathrm{pn}}^{k\tau s_z}\boldsymbol{D}_{\mathrm{n}\Omega}\right) + \boldsymbol{I}_{\mathrm{n}\Omega}^{\mathrm{T}}\left(\tilde{\boldsymbol{Z}}_{\mathrm{np}}^{k\tau s}\boldsymbol{D}_{\mathrm{p}} + \tilde{\boldsymbol{Z}}_{\mathrm{nn}}^{k\tau s}\boldsymbol{D}_{\mathrm{n}\Omega} + \tilde{\boldsymbol{Z}}_{\mathrm{nn}}^{k\tau s_z}\right) \\
\boldsymbol{\mathcal{T}}^{k\tau} &= -\boldsymbol{D}_{\mathrm{p}}^{\mathrm{T}}\left(\tilde{\boldsymbol{V}}_{\mathrm{pp}}^{k\tau s} + \tilde{\boldsymbol{V}}_{\mathrm{pn}}^{k\tau s}\right)T_s^k - \boldsymbol{D}_{\mathrm{n}\Omega}^{\mathrm{T}}\left(\tilde{\boldsymbol{V}}_{\mathrm{np}}^{k\tau s} + \tilde{\boldsymbol{V}}_{\mathrm{nn}}^{k\tau s}\right)T_s^k + \tilde{\boldsymbol{V}}_{\mathrm{np}}^{k\tau_z s}T_s^k + \tilde{\boldsymbol{V}}_{\mathrm{nn}}^{k\tau_z s}T_s^k \\
{}^{\pi}\boldsymbol{\mathcal{T}}^{k\tau} &= -\boldsymbol{I}_{\mathrm{p}}^{\mathrm{T}}\left(\tilde{\boldsymbol{V}}_{\mathrm{pp}}^{k\tau s} + \tilde{\boldsymbol{V}}_{\mathrm{pn}}^{k\tau s}\right)T_s^k - \boldsymbol{I}_{\mathrm{n}\Omega}^{\mathrm{T}}\left(\tilde{\boldsymbol{V}}_{\mathrm{np}}^{k\tau s} + \tilde{\boldsymbol{Z}}_{\mathrm{nn}}^{k\tau s}\right)T_s^k
\end{aligned}
\tag{29}
$$

Since the temperature field given in our formulation is

$$
{}^{\pi}\boldsymbol{\mathcal{T}}^{k\tau} = {}^{\pi}\overline{\boldsymbol{\mathcal{T}}}^{k\tau}
$$

the boundary conditions remain those of classical formulation given in [29]

$$
\boldsymbol{u}_{\tau}^k = \bar{\boldsymbol{u}}_{\tau}^k \quad \text{or} \quad \boldsymbol{\Pi}_{\mathrm{d}}^{k\tau s}\boldsymbol{u}_s^k = \boldsymbol{\Pi}_{\mathrm{d}}^{k\tau s}\bar{\boldsymbol{u}}_s^k \tag{30}
$$

Mixed Formulation Based on RMVT

In the mixed case, equilibrium and compatibility are both formulated in terms of the u^k and σ_{n}^k unknowns via Reissner's variational equation [35, 36, 39],

$$
\begin{aligned}
\sum_{k=1}^{N_l}\int_{\Omega^k}\int_{A_k}\Big(&\delta\varepsilon_{\mathrm{pG}}^{k^{\mathrm{T}}}\left(\sigma_{\mathrm{pH}}^k - \sigma_{\mathrm{pT}}^k\right) + \delta\varepsilon_{\mathrm{nG}}^{\mathrm{T}}\sigma_{\mathrm{nM}}^k + \\
&\delta\sigma_{\mathrm{nM}}^{k^{\mathrm{T}}}\left(\varepsilon_{\mathrm{nG}}^k - \left(\varepsilon_{\mathrm{nH}}^k - \varepsilon_{\mathrm{nT}}^k\right)\right)\Big)\,d\Omega^k\,dz = \delta L^{\mathrm{e}}
\end{aligned}
\tag{31}
$$

The left-hand side includes the variations of the internal work in the plate: the first two terms come from the displacement formulation and lead to variationally consistent equilibrium conditions; the third mixed term variationally enforces the compatibility of the transverse strain components.

Using what has been done in the previous subsection and introducing the following stress and strain layer-resultants

$$
\begin{aligned}
&\left(\boldsymbol{\mathcal{R}}_{\mathrm{pH}}^{k\tau}, \boldsymbol{\mathcal{R}}_{\mathrm{nM}}^{k\tau}, \boldsymbol{\mathcal{R}}_{\mathrm{nM}}^{k\mathrm{t}_z}, \boldsymbol{\mathcal{S}}_{\mathrm{nG}}^{k\tau}, \boldsymbol{\mathcal{S}}_{\mathrm{nH}}^{k\tau}, \boldsymbol{\mathcal{S}}_{\mathrm{nT}}^{k\tau}\right) \\
&\qquad = \int_{A_k}\left(F_\tau\sigma_{\mathrm{pH}}^k, F_\tau\sigma_{\mathrm{M}}^k, F_{\tau_z}\sigma_{\mathrm{M}}^k, F_\tau\varepsilon_{\mathrm{nG}}^k, F_\tau\varepsilon_{\mathrm{nH}}^k, F_\tau\varepsilon_{\mathrm{nT}}^k\right)dz
\end{aligned}
\tag{32}
$$

Eq. (31) leads to

$$\sum_{k=1}^{N_l}\Bigg(\int_{\Omega^k}\Big(\delta\boldsymbol{u}_\tau^{k\mathrm{T}}\Big(-\boldsymbol{D}_{\mathrm{p}}^{\mathrm{T}}\Big(\boldsymbol{\mathcal{R}}_{\mathrm{pH}}^{k\tau}-\boldsymbol{\mathcal{R}}_{\mathrm{pT}}^{k\tau}\Big)+\boldsymbol{\mathcal{R}}_{\mathrm{nM}}^{k\tau_z}-\boldsymbol{D}_{\mathrm{n}\Omega}^{\mathrm{T}}\boldsymbol{\mathcal{R}}_{\mathrm{nM}}^{k\tau}\Big)+\delta\sigma_{\mathrm{n}\tau}^{k\mathrm{T}}\big(\boldsymbol{\mathcal{S}}_{\mathrm{nG}}^{k\tau}-\big(\boldsymbol{\mathcal{S}}_{\mathrm{nH}}^{k\tau}-\boldsymbol{\mathcal{S}}_{\mathrm{nT}}^{k\tau}\big)\big)\,d\Omega$$
$$+\int_{\Gamma^k}\delta\boldsymbol{u}_\tau^{k\mathrm{T}}\Big(\boldsymbol{I}_{\mathrm{p}}^{\mathrm{T}}\Big(\boldsymbol{\mathcal{R}}_{\mathrm{pH}}^{k\tau}-\boldsymbol{\mathcal{R}}_{\mathrm{pT}}^{k\tau}\Big)+\boldsymbol{I}_{\mathrm{n}\Omega}^{\mathrm{T}}\boldsymbol{\mathcal{R}}_{\mathrm{nM}}^{k\tau}\Big)\,d\Gamma^k\Bigg)$$
$$=\sum_{k=1}^{N_l}\int_{\Omega^k}\delta\boldsymbol{u}_\tau^{k\mathrm{T}}\boldsymbol{p}_\tau^k\,d\Omega \tag{33}$$

By imposing the definition of virtual variations for the unknown stress and displacement variables, the differential system of governing equations and related boundary conditions for the k-layer are obtained in terms of the introduced stress and strain resultants.

The equilibrium equations on Ω^k are

$$\delta\boldsymbol{u}_\tau^k:\quad -\boldsymbol{D}_{\mathrm{p}}^{\mathrm{T}}\Big(\boldsymbol{\mathcal{R}}_{\mathrm{pH}}^{k\tau}-\boldsymbol{\mathcal{R}}_{\mathrm{pT}}^{k\tau}\Big)+\boldsymbol{\mathcal{R}}_{\mathrm{nM}}^{k\tau_z}-\boldsymbol{D}_{\mathrm{n}\Omega}^{\mathrm{T}}\boldsymbol{\mathcal{R}}_{\mathrm{nM}}^{k\tau}=\boldsymbol{p}_\tau^k \tag{34}$$

The constitutive equations on Ω^k are

$$\delta\sigma_{\mathrm{n}\tau}^k:\quad \boldsymbol{\mathcal{S}}_{\mathrm{nG}}^{k\tau}-\big(\boldsymbol{\mathcal{S}}_{\mathrm{nH}}^{k\tau}-\boldsymbol{\mathcal{S}}_{\mathrm{nT}}^{k\tau}\big)=0 \tag{35}$$

The boundary conditions on Γ^k are geometrical on Γ_{g}^k

$$\boldsymbol{u}_\tau^k=\bar{\boldsymbol{u}}_\tau^k \tag{36a}$$

or mechanical on Γ_{m}^k

$$\boldsymbol{I}_{\mathrm{p}}^{\mathrm{T}}\boldsymbol{\mathcal{R}}_{\mathrm{pH}}^{k\tau}+\boldsymbol{I}_{\mathrm{n}\Omega}^{\mathrm{T}}\boldsymbol{\mathcal{R}}_{\mathrm{nM}}^{k\tau}=\boldsymbol{I}_{\mathrm{p}}^{\mathrm{T}}\bar{\boldsymbol{\mathcal{R}}}_{\mathrm{pH}}^{k\tau}+\boldsymbol{I}_{\mathrm{n}\Omega}^{\mathrm{T}}\bar{\boldsymbol{\mathcal{R}}}_{\mathrm{nM}}^{k\tau} \tag{36b}$$

Thermal contributions to the boundary condition have been omitted for the same reason discussed in the classical displacement formulation.

In order to express the governing equations in terms of stress and displacement variables, the extra resultants in Eq. (19) are written in terms of the unknown variables using Eqs. (4), (7), (9), and (18),

$$\begin{aligned}&\boldsymbol{\mathcal{R}}_{\mathrm{pH}}^{k\tau}=\boldsymbol{Z}_{\mathrm{pp}}^{k\tau s}\boldsymbol{D}_{\mathrm{p}}\boldsymbol{u}_s^k+\boldsymbol{Z}_{\mathrm{pn}}^{k\tau s}\sigma_{\mathrm{n}s}^k\quad \boldsymbol{\mathcal{R}}_{\mathrm{nM}}^{k\tau}=E_{\tau s}^k\sigma_{\mathrm{n}s}^k\quad \boldsymbol{\mathcal{R}}_{\mathrm{nM}}^{k\tau_z}=E_{\tau_z s}\sigma_{\mathrm{n}s}^k\\&\boldsymbol{\mathcal{S}}_{\mathrm{nG}}^{k\tau}=E_{\tau s}^k\boldsymbol{D}_{\mathrm{n}\Omega}\boldsymbol{u}_s^k+E_{\tau s_z},\boldsymbol{u}_s^k\quad \boldsymbol{\mathcal{S}}_{\mathrm{nH}}^{k\tau}=\boldsymbol{Z}_{\mathrm{np}}^{k\tau s}\boldsymbol{D}_{\mathrm{p}}\boldsymbol{u}_s^k+\boldsymbol{Z}_{\mathrm{nn}}^{k\tau s}\sigma_{\mathrm{n}s}^k\quad \boldsymbol{\mathcal{S}}_{\mathrm{nT}}^{k\tau}=E_{\tau s}^k\alpha_{\mathrm{n}}^k T_s^k\end{aligned} \tag{37}$$

Further layer-stiffnesses and integrals have been introduced

$$(\boldsymbol{Z}_{\mathrm{pp}}^{k\tau s},\boldsymbol{Z}_{\mathrm{pn}}^{k\tau s},\boldsymbol{Z}_{\mathrm{np}}^{k\tau s},\boldsymbol{Z}_{\mathrm{nn}}^{k\tau s})=(\boldsymbol{C}_{\mathrm{pp}}^k,\boldsymbol{C}_{pn}^l,\boldsymbol{C}_{\mathrm{np}}^k,\boldsymbol{C}_{\mathrm{nn}}^k)E_{\tau s} \tag{38}$$

The governing equations expressed in terms of displacement and stress variables are

$$\begin{aligned} \delta \boldsymbol{u}_\tau^k: \quad & \boldsymbol{K}_{uu}^{k\tau s}\boldsymbol{u}_s^k + \boldsymbol{K}_{u\sigma}^{k\tau s}\sigma_{\mathrm{n}s}^k = \boldsymbol{p}_\tau^k + {}^u\boldsymbol{\mathcal{T}}^{k\tau} \\ \delta \sigma_{\mathrm{n}\tau}^k: \quad & \boldsymbol{K}_{\sigma u}^{k\tau s}\boldsymbol{u}_s^k + \boldsymbol{K}_{\sigma}^{k\tau s}\sigma_{\mathrm{n}s}^k = {}^\sigma\boldsymbol{\mathcal{T}}^{k\tau} \end{aligned} \tag{39}$$

with boundary conditions

$$\boldsymbol{u}_\tau^k = \bar{\boldsymbol{u}}_\tau^k \quad \text{or} \quad \boldsymbol{\Pi}_u^{k\tau s}\boldsymbol{u}_s^k + \boldsymbol{\Pi}_\sigma^{k\tau s}\sigma_{\mathrm{n}s}^k = \boldsymbol{\Pi}_u^{k\tau s}\bar{\boldsymbol{u}}_s^k + \boldsymbol{\Pi}_\sigma^{k\tau s}\bar{\sigma}_{\mathrm{n}s}^k \tag{40}$$

where

$$\begin{aligned} \boldsymbol{K}_{uu}^{k\tau s} &= \boldsymbol{D}_{\mathrm{p}}^{\mathrm{T}}\boldsymbol{Z}_{\mathrm{pp}}^{k\tau s}\boldsymbol{D}_{\mathrm{p}} & \boldsymbol{K}_{u\sigma}^{k\tau s} &= -\boldsymbol{D}_{\mathrm{p}}^{\mathrm{T}}\boldsymbol{Z}_{\mathrm{pn}}^{k\tau s} + E_{\tau_z s}\boldsymbol{I} - E_{\tau s}\boldsymbol{D}_{\mathrm{n}\Omega}^{\mathrm{T}} \\ \boldsymbol{K}_{\sigma u}^{k\tau s} &= \boldsymbol{E}_{\tau s}\boldsymbol{D}_{\mathrm{n}\Omega} + E_{\tau s_z}\boldsymbol{I} - \boldsymbol{Z}_{\mathrm{np}}^{k\tau s}\boldsymbol{D}_{\mathrm{p}} & \boldsymbol{K}_{\sigma\sigma}^{k\tau s} &= -\boldsymbol{Z}_{\mathrm{nn}}^{k\tau s} \\ \boldsymbol{\Pi}_u^{k\tau s} &= \boldsymbol{I}_{\mathrm{p}}^{\mathrm{T}}\boldsymbol{Z}_{\mathrm{pp}}^{k\tau s}\boldsymbol{D}_{\mathrm{p}} & \boldsymbol{\Pi}_\sigma^{k\tau s} &= \boldsymbol{Z}_{\mathrm{pn}}^{k\tau s} + E_{\tau s}\boldsymbol{I}_{\mathrm{n}\Omega}^{\mathrm{T}} \\ {}^u\boldsymbol{\mathcal{T}}^{k\tau} &= -\boldsymbol{D}_{\mathrm{p}}^{\mathrm{T}}(\tilde{\boldsymbol{V}}_{\mathrm{pp}}^{k\tau s} + \tilde{\boldsymbol{V}}_{\mathrm{pn}}^{k\tau s})T_s^k & {}^\sigma\boldsymbol{\mathcal{T}}^{k\tau} &= E_{\tau s}^k\alpha_{\mathrm{n}}^k T_s^k \end{aligned} \tag{41}$$

With respect to the case of pure mechanical loadings examined in the author's previous work, the constitutive equations appear in a nonhomogeneous form. Such nonhomogeneous terms are zero if and only if α_{n}^k is zero, as is the case discussed in the present article.

FULFILLMENT OF C_z^0-REQUIREMENTS, MULTILAYERED EQUATIONS, AND CLOSED-FORM SOLUTION

The C_z^0-requirements Eqs. (12), (13), and (16) can be accounted for by simply writing the governing equations at the multilayered level. The necessary steps have been extensively explained in the author's previous works [7, 27, 29].

By choosing the top and N r-variables as layer unknowns, the arrays of the unknown displacements for the whole multilayer holds:

$$\begin{aligned} \boldsymbol{u}^{\mathrm{T}} = \{ & \boldsymbol{u}_{\mathrm{b}}^{1^{\mathrm{T}}}, \boldsymbol{u}_{\mathrm{t}}^{1^{\mathrm{T}}}, \boldsymbol{u}_2^{1^{\mathrm{T}}}; \boldsymbol{u}_{\mathrm{t}}^{2^{\mathrm{T}}}, \boldsymbol{u}_2^{2\mathrm{T}}; \ldots, \boldsymbol{u}_{\mathrm{t}}^{k^{\mathrm{T}}}, \boldsymbol{u}_2^{k^{\mathrm{T}}}; \\ & \boldsymbol{u}_{\mathrm{t}}^{(k+1)^{\mathrm{T}}}, \boldsymbol{u}_2^{(k+1)^{\mathrm{T}}}; \ldots, \boldsymbol{u}_{\mathrm{t}}^{(N_l-1)^{\mathrm{T}}}, \boldsymbol{u}_2^{(N_l-1)^{\mathrm{T}}}; \boldsymbol{u}_{\mathrm{t}}^{(N_l)^{\mathrm{T}}}, \boldsymbol{u}_2^{(N_l)^T}\} \end{aligned} \tag{42}$$

The governing equations for the displacement formulation are formally written as

$$\boldsymbol{K}_{\mathrm{d}}\boldsymbol{u} = \boldsymbol{p}$$

$$\boldsymbol{u} = \bar{\boldsymbol{u}} \quad \text{or} \quad \boldsymbol{\Pi}_{\mathrm{d}}\boldsymbol{u} = \boldsymbol{\Pi}_{\mathrm{d}}\bar{\boldsymbol{u}} \tag{43}$$

where the vector $\boldsymbol{p}$ includes thermal and mechanical loadings. By introducing a stress array for the whole multilayer

$$\begin{aligned} \sigma_{\mathrm{n}}^{\mathrm{T}} = \{ & \sigma_{\mathrm{nt}}^{1^{\mathrm{T}}}, \sigma_{\mathrm{n2}}^{1^{\mathrm{T}}}; \sigma_{\mathrm{nt}}^{2^{\mathrm{T}}}, \sigma_{\mathrm{n2}}^{2^{\mathrm{T}}}; \ldots, \sigma_{\mathrm{nt}}^{k^{\mathrm{T}}}, \sigma_{\mathrm{n2}}^{k^{\mathrm{T}}}; \\ & \sigma_{\mathrm{nt}}^{(k+1)^{\mathrm{T}}}, \sigma_{\mathrm{n2}}^{(k+1)^{\mathrm{T}}}; \ldots, \sigma_{\mathrm{nt}}^{(N_l-1)^{\mathrm{T}}}, \sigma_{\mathrm{n2}}^{(N_l-1)^{\mathrm{T}}}; \sigma_{\mathrm{n2}}^{N_l^{\mathrm{T}}}\} \end{aligned} \tag{44}$$

the governing system of differential equations at the multilayer level for the mixed cases is formally written in final form as

$$\begin{aligned} \boldsymbol{K}_{uu}\boldsymbol{u} + \boldsymbol{K}_{u\sigma}\sigma_{\mathrm{n}} &= \boldsymbol{p} + \boldsymbol{p}_u^{1N_l} \\ \boldsymbol{K}_{\sigma u}\boldsymbol{u} + \boldsymbol{K}_{\sigma\sigma}\sigma_{\mathrm{n}} &= \boldsymbol{p}_\sigma^{1N_l} \end{aligned} \tag{45}$$

Here $\boldsymbol{p}_u^{1N_l}$, $\boldsymbol{p}_\sigma^{1N_l}$ are loadings due to the nonhomogeneous conditions in the equilibrium and/or constitutive equations. The boundary conditions are

$$\boldsymbol{u} = \bar{\boldsymbol{u}} \quad \text{or} \quad \boldsymbol{\Pi}_u\boldsymbol{u} + \boldsymbol{\Pi}_\sigma\sigma_{\mathrm{n}} = \boldsymbol{\Pi}_u\bar{\boldsymbol{u}} + \boldsymbol{\Pi}_\sigma\bar{\sigma}_{\mathrm{n}} + \boldsymbol{q}_\sigma^{1N_l} \tag{46}$$

The expanded expressions of the multilayer governing equations have been omitted for the sake of brevity. Exact, closed-form solutions of the derived system of differential equations (43), (45), and (46), which govern the thermomechanical response of a generally laminated multilayered plate, are not available. Approximate solution procedures could be conveniently implemented for this purpose [7]. The particular case in which the material has the properties $\tilde{C}_{16} = \tilde{C}_{26} = \tilde{C}_{36} = \tilde{C}_{45} = 0$ has been considered here. In such a case, Navier-type closed-form solutions can be found by assuming the following harmonic forms for the applied mechanical and thermal loadings and unknown variables,

$$\begin{aligned} (u_{x_\tau}^k, \sigma_{xz_\tau}^k, p_{x_\tau}^k) &= \sum_{m,n} (U_{x_\tau}^k, S_{xz_\tau}^k, P_{x_\tau}^k) \cos\frac{m\pi x}{a} \sin\frac{n\pi y}{b} \\ (u_{y_\tau}^k, \sigma_{yz_\tau}^k, p_{y_\tau}^k) &= \sum_{m,n} (U_{y_\tau}^k, S_{yz_\tau}^k, P_{y_\tau}^k) \sin\frac{m\pi x}{a} \cos\frac{n\pi y}{b} \\ (u_{z_\tau}^k, \sigma_{zz_\tau}^k, p_{z_\tau}^k) &= \sum_{m,n} (U_{z_\tau}^k, S_{zz_\tau}^k, P_{z_\tau}^k) \sin\frac{m\pi x}{a} \sin\frac{n\pi y}{b} \end{aligned} \tag{47}$$

$$T = T_0(z) \sin\frac{m\pi x}{a} \sin\frac{n\pi y}{b}$$

which correspond to simply supported boundary conditions. a and b are the plate lengths in the x- and y-directions, respectively; m and n are the corresponding wave numbers; and capital letters on the right-hand side denote corresponding maximum amplitudes. Upon substituting Eqs. (47), the governing equations assume the form of a linear system of algebraic equation whose solutions are discussed in the next paragraph.

NUMERICAL ILLUSTRATIONS

In order to compare the accuracy of the considered mixed and classical models to the static response of simply supported, orthotropic laminated plates, subjected to an in-plane harmonic distribution of temperature loadings, a comprehensive numerical investigation related to thick and thin cross-ply laminated plates was conducted.

Some of the most important results are discussed in the following text. The previously introduced acronyms are used extensively to denote the implemented theories.

Most of the analyses presented refer to a thermomechanical problem for which the three-dimensional exact solution was recently given by Bhaskar et al. [6]. Numerical results are presented for two geometries:

1. a cylindrically bent plate loaded by a temperature field given by

$$T = T_0 \frac{2z}{h} \sin \frac{\pi x}{a}$$

2. a square plate loaded by a temperature field given by

$$T = T_0 \frac{2z}{h} \sin \frac{\pi x}{a} \sin \frac{\pi y}{b}$$

The mechanical properties of the lamina are

$$\frac{E_L}{E_T} = 25, \qquad \frac{G_{LT}}{E_T} = 0.5, \qquad \frac{G_{TT}}{E_T} = 0.2,$$

$$\frac{\nu_{LT}}{\nu_{TT}} = 0.25, \qquad \frac{\alpha_T}{\alpha_L} = 1125$$

where L and T refer to directions parallel and perpendicular, respectively, to the fibers (see [11] for notation).

The problems of Bhaskar et al. are addressed in Tables 1–3 and Figures 4–10. Unsymmetrically laminated plates are considered in Table 4, while a brief insight into the effects of through-the-thickness temperature distribution $T(z)$ is considered in Table 5, where constant and linear cases are compared.

In-plane and out-of-plane responses are compared for thin and thick plate geometries. The deflection and stresses are presented in terms of the dimensionless parameters

$$\bar{U}_z = h u_z/(\alpha_L T_0 a^2) \qquad (\bar{U}_x \bar{U}_y) = (u_x, u_y)/(\alpha_L T_0 a) \qquad \bar{S}_{ij} = \sigma_{ij}/(E_T \alpha_L T_0)$$

In contrast to the author's previous analyses, where the plate response to mechanical loadings was investigated, it has been found that an accurate description of transverse normal stress requires the integration of three-dimensional equilibrium equations. Therefore, all the depicted transverse normal stress results are those obtained by integration of the three-dimensional equilibrium equations, while transverse shear components are those directly given by the assumed model of Eqs. (9). The LM4 results are used as a reference solution for those plots and tables for which an exact analysis is not available. The following main comments can be made on the reported results.

Table 1 Influence of thickness ratio on the accuracy of the considered theories for the cylindrical bending problem considered by Bhaskar et al. [6]; three-layered plate $0^\circ/0^\circ/0^\circ$

(*a*) In-plane displacement $\bar{U}_x$ at $z = \mp h/2$

a/h	2	4	10	20	50	100
Exact	±13.38	±7.470	±5.009	±4.589	±4.467	±4.449
LM4	±13.37	±7.461	±5.009	±4.589	±4.467	±4.449
LM3	±11.62	±7.169	±5.975	±4.581	±4.466	±4.449
LM2	±10.13	±7.116	±5.015	±4.594	±4.466	±4.449
LM1	±8.686	±5.760	±5.057	±4.675	±4.558	±4.540
LD4	±13.37	±7.469	±5.009	±4.589	±4.467	±4.449
LD3	±13.28	±7.467	±5.009	±4.589	±4.467	±4.449
LD2	±12.35	±7.345	±5.001	±4.587	±4.467	±4.449
LD1	±7.327	±6.136	±5.311	±5.147	±5.099	±5.092
EMZC3	±12.46	±7.388	±5.007	±4.589	±4.467	±4.449
EMZC2	±5.994	±5.192	±4.606	±4.486	±4.450	±4.450
EMZC1	±4.374	±5.587	±6.488	±6.673	±6.728	±6.736
EMC4	±11.32	±7.374	±5.025	±4.594	±4.468	±4.449
EMC3	±10.96	±7.281	±5.015	±4.592	±4.468	±4.450
EMC2	±4.489	±4.454	±4.445	±4.444	±4.444	±4.443
EMC1	±6.739	±6.739	±6.739	±6.739	±6.739	±6.739
EDZ3	±12.83	±7.416	±5.046	±4.588	±4.467	±4.449
EDZ2	±6.202	±5.268	±4.617	±4.489	±4.451	±4.445
EDZ1	±4.263	±5.581	±6.494	±6.674	±6.728	±6.736
ED4	±12.21	±7.570	±5.044	±4.598	±4.468	±4.449
ED3	±12.22	±7.566	±5.044	±4.598	±4.468	±4.450
ED2	±4.531	±4.465	±4.447	±4.445	±4.444	±4.443
ED1	±10.59	±10.59	±10.59	±10.59	±10.59	±10.59
CLT	±4.444	±4.444	±4.444	±4.444	±4.444	±4.444

Table 1 *cont.*
(*b*) Transverse displacement $\bar{U}_z$ at $z = \mp h/2$

a/h	2	4	10	20	50	100
Exact	61.12	18.32	5.408	3.479	2.933	2.855
LM4	61.12	18.32	5.408	3.479	2.933	2.855
LM3	61.22	18.33	5.408	3.479	2.933	2.855
LM2	61.82	18.35	5.408	3.479	2.933	2.855
LM1	55.43	17.55	5.433	3.535	2.991	2.913
LD4	61.17	18.32	5.408	3.479	2.933	2.855
LD3	61.06	18.32	5.408	3.479	2.933	2.855
LD2	59.97	18.20	5.401	3.478	2.933	2.855
LD1	51.34	16.10	5.381	3.779	3.326	3.262
EMZC3	60.85	18.30	5.405	3.478	2.933	2.855
EMZC2	59.18	17.50	5.235	3.434	2.926	2.853
EMZC1	4.374	5.587	6.488	6.672	6.728	6.736
EMC4	62.39	18.91	5.508	3.503	2.937	2.855
EMC3	62.88	18.94	5.509	3.504	2.937	2.856
EMC2	59.24	17.00	5.100	3.397	2.920	2.852
EMC1	6.739	6.739	6.739	6.739	6.739	6.739
EDZ3	60.49	18.27	5.408	3.478	2.933	2.855
EDZ2	56.71	16.99	5.161	3.415	2.923	2.853
EDZ1	4.263	5.581	6.494	6.674	6.728	6.736
ED4	62.31	18.98	5.517	3.505	2.937	2.856
ED3	62.31	18.98	5.517	3.505	2.937	2.856
ED2	54.21	15.81	4.912	3.350	2.912	2.850
ED1	6.739	6.739	6.739	6.739	6.739	6.739
CLT	2.829	2.829	2.829	2.829	2.829	2.829

Table 1 ***cont.***
(*c*) In-plane stress $\bar{S}_{xx}$ at $z = \mp h/6$ (first and third layers)

a/h	2	4	10	20	50	100
Exact	±369.7	±372.3	±371.7	±371.5	±371.4	±371.4
LM4	±370.4	±372.3	±371.7	±371.4	±371.3	±371.3
LM3	±368.0	±371.8	±371.6	±371.4	±371.3	±371.3
LM2	±371.4	±372.1	±371.6	±371.4	±371.3	±371.3
LM1	±517.3	±508.7	±500.8	±499.0	±498.4	±498.4
LD4	±369.7	±372.3	±371.7	±371.4	±371.3	±371.3
LD3	±370.7	±372.5	±371.7	±371.4	±371.3	±371.3
LD2	±368.1	±372.2	±371.8	±371.4	±371.3	±371.3
LD1	±507.7	±502.3	±498.7	±498.0	±497.8	±497.7
EMZC3	±367.0	±371.9	±371.7	±371.5	±371.4	±371.4
EMZC2	±379.6	±375.1	±372.2	±371.6	±371.5	±371.4
EMZC1	±483.3	±487.5	±490.7	±491.4	±491.16	±491.6
EMC4	±382.8	±375.7	±372.2	±371.6	±371.5	±371.4
EMC3	±382.0	±375.8	±372.3	±371.7	±371.5	±371.4
EMC2	±372.2	±371.6	±371.5	±371.4	±371.4	±371.4
EMC1	±491.6	±491.6	±491.6	±491.6	±491.6	±491.6
EDZ3	±366.9	±372.0	±371.8	±371.5	±371.4	±371.4
EDZ2	±380.9	±372.3	±371.7	±371.5	±371.5	±371.4
EDZ1	±483.7	±487.9	±490.8	±491.4	±491.6	±491.6
ED4	±384.1	±376.0	±372.3	±371.6	±371.5	±371.4
ED3	±384.0	±376.2	±372.3	±371.7	±371.5	±371.5
ED2	±373.2	±371.9	±371.5	±371.5	±371.4	±371.4
ED1	±491.6	±491.6	±491.6	±491.6	±491.6	±491.6
CLT	±371.4	±371.4	±371.4	±371.4	±371.4	±371.4

Table 1 *cont.*
(*d*) Transverse shear stress $\bar{S}_{xz}$ at $z = h/6$

a/h	2	4	10	20	50	100
Exact	−3.508	2.830	2.580	1.441	0.5948	0.2987
LM4	−3.490	2.831	2.580	1.441	0.5947	0.2987
LM3	−3.236	2.845	2.580	1.441	0.5947	0.2987
LM2	−2.062	3.004	2.586	1.442	0.5947	0.2987
LM1	2.780	8.968	6.314	3.464	1.423	0.7144
LD4	−3.521	2.830	2.580	1.441	0.5947	0.2987
LD3	−3.414	2.832	2.579	1.441	0.5947	0.2987
LD2	−6.030	2.306	2.545	1.437	0.5944	0.2987
LD1	15.17	12.195	6.189	3.225	1.305	0.6538
EMZC3	−3.814	2.840	2.589	1.443	0.5950	0.2987
EMZC2	3.050	4.535	2.735	1.462	0.5962	0.2990
EMZC1	34.07	13.37	4.263	2.020	0.7946	0.3963
EMC4	−16.80	0.6969	2.453	1.426	0.5940	0.2987
EMC3	−15.10	0.9014	2.461	1.427	0.5940	0.2987
EMC2	14.99	7.484	2.992	1.496	0.5984	0.2992
EMC1	19.80	9.901	3.960	1.980	0.7920	0.3960
EDZ3	−4.814	2.687	2.580	1.442	0.5949	0.2988
EDZ2	1.544	4.271	2.719	1.460	0.5961	0.2989
EDZ1	33.44	13.09	4.230	2.015	0.7943	0.3963
ED4	−20.91	0.2463	2.436	1.425	0.5938	0.2987
ED3	−20.92	0.2403	2.434	1.424	0.5938	0.2987
ED2	15.03	7.489	2.993	1.496	0.5984	0.2992
ED1	19.80	9.900	3.960	1.980	0.7920	0.3960
CLT	14.95	7.479	2.991	1.495	0.5981	0.2985

Table 1 ***cont.***
(*e*) Transverse normal stress $\bar{S}_{zz}$ at $z = h/6$

a/h	2	4	10	20	50	100
Exact	±9.233	±1.748	±0.2044	±0.0471	±0.0073	±0.0018
LM4	±9.470	±1.759	±0.2046	±0.0471	±0.0073	±0.0018
LM3	±13.40	±2.575	±0.3072	±0.0712	±0.0111	±0.0027
LM2	±14.67	±2.706	±0.3092	±0.0708	±0.0110	±0.0027
LM1	±52.96	±17.29	±9.292	±5.874	±5.475	±5.418
LD4	±9.236	±1.748	±0.2044	±0.0471	±0.0073	±0.0018
LD3	±9.212	±1.747	±0.2044	±0.0471	±0.0074	±0.0018
LD2	±9.988	±1.824	±0.2064	±0.0472	±0.0074	±0.0018
LD1	±7.629	±1.274	±0.1317	±0.0294	±0.0045	±0.1125
EMZC3	±10.79	±1.960	±0.2235	±0.0513	±0.0080	±0.0020
EMZC2	±12.86	±2.665	±0.3594	±0.0864	±0.0137	±0.0034
EMZC1	±2.770	±1.349	±0.2938	±0.0775	±0.0126	±0.0032
EMC4	±7.972	±1.097	±0.0902	±0.0186	±0.0028	±0.0007
EMC3	±9.597	±1.354	±0.1130	±0.0234	±0.0035	±0.0009
EMC2	±18.32	±4.604	±0.7376	±0.1845	±0.0295	±0.0074
EMC1	0.0	0.0	0.0	0.0	0.0	0.0
EDZ3	±9.682	±1.777	±0.2047	±0.0471	±0.0074	±0.0018
EDZ2	±8.300	±1.586	±0.1979	±0.0467	±0.0073	±0.0018
EDZ1	±2.295	±1.073	±0.2271	±0.0595	±0.0097	±0.0024
ED4	±5.892	±0.7768	±0.0611	±0.0125	±0.0019	±0.0005
ED3	±5.895	±0.7672	±0.0611	±0.0125	±0.0019	±0.0005
ED2	±10.55	±2.667	±0.4280	±0.1070	±0.0171	±0.0043
ED1	0.0	0.0	0.0	0.0	0.0	0.0
CLT	0.0	0.0	0.0	0.0	0.0	0.0

Table 2 Influence of thickness ratio on the accuracy of the considered theories for the square plate problem considered by Bhaskar et al. [6]; three-layered plate $0^\circ/90^\circ/0^\circ$

	U_z at $z = \mp h/2$		S_{xz} at $z = \mp h/6$		S_{zz} at $z = \mp h/6$	
a/h	4	100	4	100	4	100
Exact	42.69	10.26	84.81	7.073	±0.5786	±0.1738E-5
LM4	42.69	10.26	84.81	7.073	0.6092	0.1297E-5
					−0.5002	−0.1167E-5
LM3	42.70	10.26	84.85	7.073	1.611	0.1242E-5
					2.717	0.2495E-2
LM2	42.74	10.26	84.90	7.073	2.716	0.1188E-2
					4.787	0.2378E-2
LM1	42.62	10.33	94.74	7.498	−5.303	−0.1560E-1
					4.894	−0.1790E-1
LD4	42.69	10.26	84.81	7.073	0.5783	0.1253E-5
					0.5783	−0.1253E-5
LD3	42.68	10.26	84.82	7.073	0.5781	0.1253E-5
					0.5781	−0.1254E-5
LD2	42.25	10.26	82.92	7.073	0.6075	0.1453E-5
					0.6075	−0.1453E-5
LD1	41.24	10.92	235.4	7.672	−0.1463	−0.1132E-2
					0.1463	0.1133E-2
EMZC3	42.44	10.26	83.81	7.073	0.9144	0.4264E-2
					0.8088	0.9414E-3
EMZC2	41.99	10.26	89.04	7.074	1.600	0.1024E-2
					2.402	0.1890E-2
EMZC1	36.96	16.12	116.3	9.198	−2.046	−0.1950E-2
					0.8202	−0.5823E-2
ED4	42.05	10.25	88.64	7.075	7.651	0.0212
					−7.651	−0.0212
ED3	42.04	10.25	88.62	7.075	7.651	0.0212
					−7651	−0.0212
ED2	34.74	10.23	116.2	7.079	18.56	0.0398
					−18.56	−0.0398
ED1	30.42	16.09	144.2	9.204	15.03	0.0391
					−15.03	−0.0391
CLT	10.18	10.18	177.13	7.089	—	—

Table 3 Influence of thickness ratio on U_z at $z = \mp h/2$ – a comparison of the considered theories; unsymmetrically laminate square plate problem
(*a*) Two layers $0^\circ/90^\circ$

a/h	2	4	10	20	50	100
LM4	96.55	52.10	38.09	35.97	35.36	35.28
LM3	97.41	98.17	98.17	35.97	35.36	35.28
LM2	98.17	52.23	38.10	35.97	35.36	35.28
LM1	91.63	51.70	38.11	35.97	35.36	35.28
LD4	96.45	52.09	38.09	35.96	35.36	35.28
LD3	96.34	52.09	38.09	35.96	35.36	35.28
LD2	91.58	50.04	37.67	35.85	35.34	35.27
LD1	80.89	50.42	40.67	39.20	38.78	38.72
EMZC3	94.59	51.00	37.84	35.90	35.35	35.27
EMZC2	96.41	52.18	38.11	35.97	35.36	35.28
EMZC1	90.37	52.18	39.92	38.05	35.51	37.44
EMC4	97.34	52.27	38.11	35.97	35.36	35.27
EMC3	98.61	52.19	38.04	35.95	35.35	35.27
EMC2	98.16	52.40	38.14	35.98	35.36	35.27
EMC1	47.89	47.89	47.89	47.89	47.89	47.88
EDZ3	93.06	50.47	37.74	35.87	35.35	35.27
EDZ2	90.90	50.36	35.77	35.88	35.35	35.27
EDZ1	80.89	50.42	40.67	39.20	38.78	38.72
ED4	97.29	52.32	38.12	35.97	35.36	35.27
ED3	96.07	51.27	37.86	35.90	35.35	35.27
ED2	89.99	49.93	37.67	35.85	35.34	35.26
ED1	47.89	47.89	47.89	47.89	47.89	47.89
ED1-CLT	35.26	35.25	35.25	35.25	35.25	35.25

Table 3 *cont.*
(*b*) Four layers $0^\circ/90^\circ/0^\circ/90^\circ$

a/h	2	4	10	20	50	100
LM4	94.52	38.21	17.62	14.30	13.35	13.21
LM3	94.57	38.21	17.62	14.30	13.35	13.21
LM2	94.89	38.23	17.62	14.30	13.35	13.21
LM1	93.21	37.50	17.50	14.27	13.34	13.21
LD4	94.52	38.21	17.62	14.30	13.35	13.21
LD3	94.50	38.21	17.62	14.30	13.35	13.21
LD2	93.36	38.08	17.61	14.30	13.35	13.21
LD1	89.40	36.77	17.68	14.64	13.76	13.64
EMZC3	93.47	37.02	17.31	14.22	13.33	13.21
EMZC2	75.48	30.31	16.04	13.89	13.28	13.19
EMZC1	28.35	20.69	18.86	18.62	18.55	18.54
EMC4	96.47	37.92	17.44	14.25	13.34	13.21
EMC3	94.36	36.13	17.02	14.31	13.32	13.20
EMC2	76.40	30.10	15.95	13.87	13.28	13.20
EMC1	19.89	19.89	19.89	19.89	19.89	19.89
EDZ3	93.20	36.81	17.25	14.20	13.33	13.21
EDZ2	72.59	29.42	15.88	13.85	13.27	13.19
EDZ1	26.10	20.31	18.97	18.80	18.75	18.74
ED4	96.52	37.74	17.39	13.21	13.34	13.21
ED3	93.26	35.58	16.90	14.11	13.32	13.20
ED2	71.99	28.82	15.73	13.81	13.27	13.19
ED1	19.89	19.89	19.89	19.89	19.89	19.89
ED1-CLT	13.16	13.16	13.16	13.16	13.16	13.16

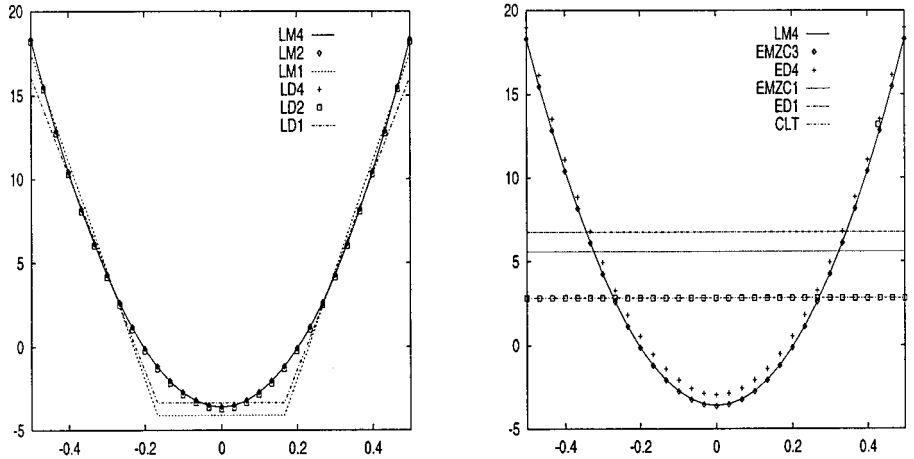

Figure 5. $\bar{U}_z$ vs z: LW (left) and ESLM (right) thick plate $a/h = 4$; cylindrical bending problem.

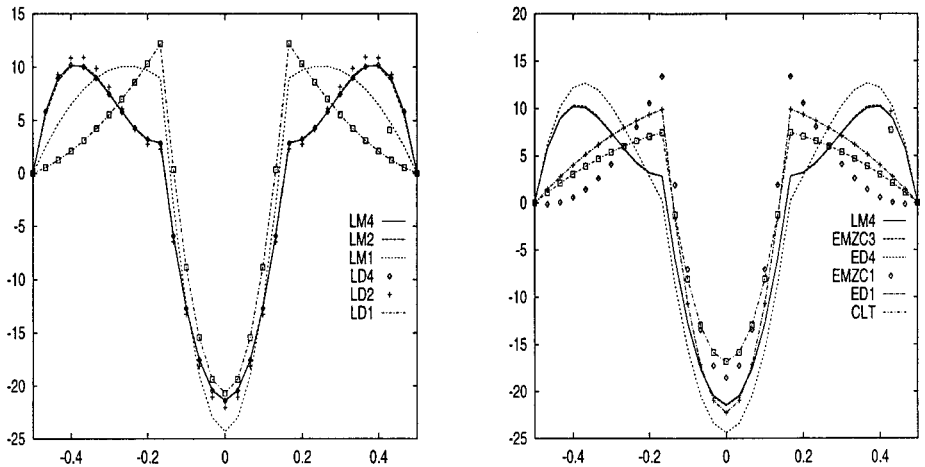

Figure 6. S_{xz} (from 3D) vs z: LW (left) and ESLM (right) thick plate $a/h = 4$; cylindrical bending.

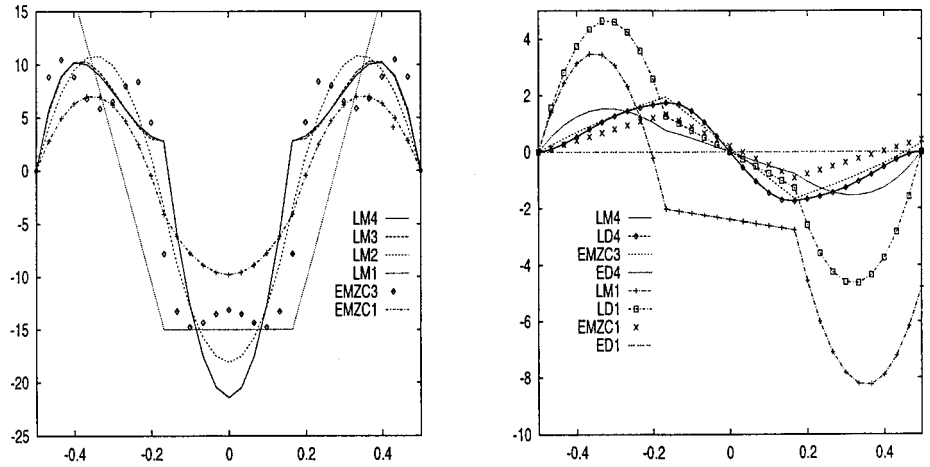

Figure 7. S_{xz} (a priori left from 3D right) vs z: LW and ESLM results for thick plate $a/h = 4$; cylindrical bending problem.

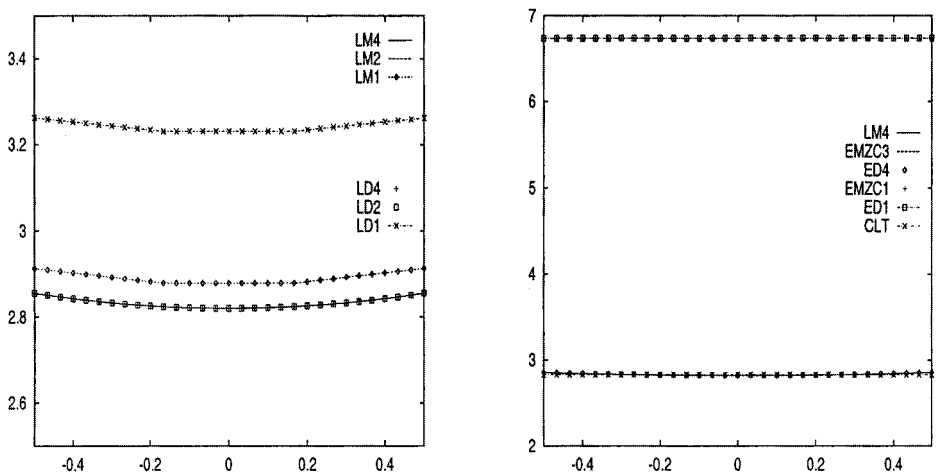

Figure 8. $\bar{U}_z$ vs z: LW (left) and ELSM (right) thin plate $a/h = 100$; cylindrical bending problem.

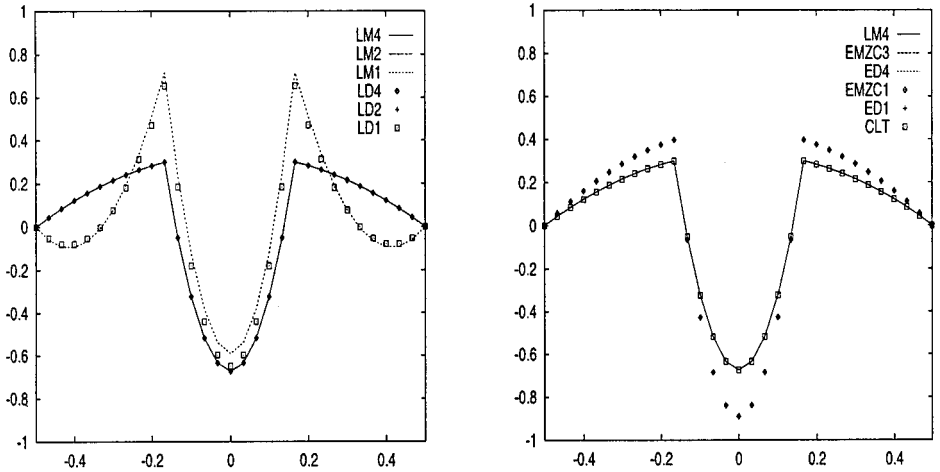

Figure 9. S_{xz} (from 3D) vs z: LW (left) and ESLM (right) thin plate $a/h = 4$; cylindrical bending problem.

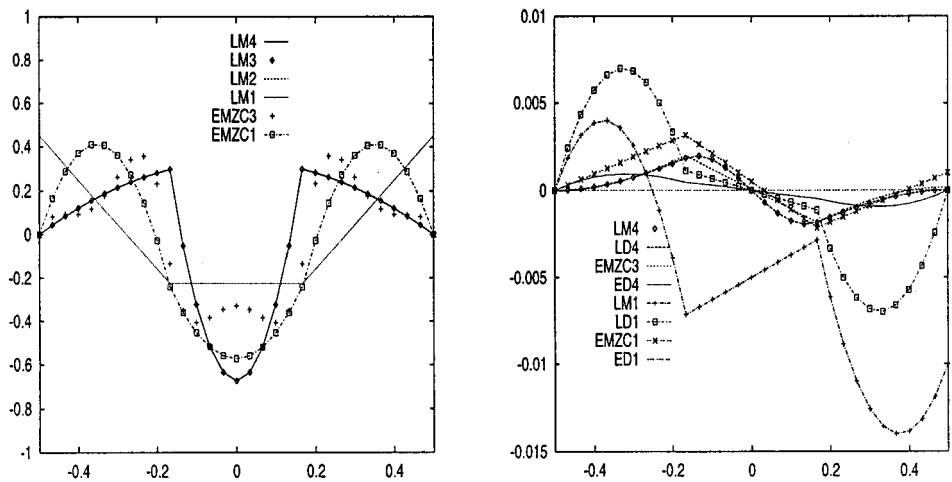

Figure 10. S_{xz} (left, a priori) and S_{zz} (right, from 3D) vs z: LW and ESLM results for thin plate $a/h = 100$; cylindrical bending problem.

Table 4 Through-the-thickness temperature distribution effects on the accuracy of transverse displacements amplitude $\bar{U}_z$ at $z = h/2$

a/h	2	4	10	20	50	100
			Constant distribution case			
LD4	−164.2	−43.23	−6.700	−1.750	−0.2800	−0.0700
LD2	−163.8	−43.22	−6.700	−1.750	−0.2800	−0.0700
LD1	−163.7	−43.22	−6.700	−1.750	−0.2800	−0.0700
ED4	−165.2	−43.29	−6.991	−1.750	−0.2800	−0.0700
ED2	−164.5	−43.30	−6.992	−1.750	−0.2800	−0.0700
ED1	−159.9	−42.75	−6.974	−1.749	−0.2800	−0.0700
ED1-CLT	0.0	0.0	0.0	0.0	0.0	0.0
			Linear distribution case			
Exact	61.12	18.32	5.408	3.479	2.933	2.855
LD4	61.17	18.32	5.408	3.479	2.933	2.855
LD2	59.97	18.20	5.401	3.478	2.933	2.855
LD1	51.34	16.10	5.381	3.779	3.326	3.262
ED4	62.31	18.98	5.517	3.505	2.937	2.856
ED2	54.21	15.81	4.912	3.350	2.912	2.850
ED1	6.739	6.739	6.739	6.739	6.739	6.739
ED1-CLT	2.829	2.829	2.829	2.829	2.829	2.829

Layer-wise analyses lead to excellent agreement with exact three-dimensional solutions. A higher order expansion should be used in each layer for very thick plate cases. Better results are obtained for mixed LM theories with respect to LD cases. Such a result confirms the effectiveness of Reissner's theorem to analyze multilayered structures. LW description results are more accurate than the related ESL results. Such a superiority is more evident for N_l increasing and for unsymmetrically laminated plates. The accuracy of the different theories is very much subordinate to the chosen expansion, that is, the N-value. Figures 5–10 show that such accuracy could be significantly subordinate to the z-position. Different theories can furnish very different accuracies, depending on the considered parameters and variables: in-plane stresses are better approximated than out-of-plane stresses; in some cases, the sign of transverse shear stresses can be wrongly predicted.

Table 3 and Figures 7 and 10 show that inescapable errors involved in the integration of the three-dimensional equilibrium equations (which consist of a post-processing procedure) can lead to the violation of zero-bottom homogeneous conditions for the transverse normal stresses. This fact becomes more evident for decreasing N as well as in the ESL implementations.

One should note that LM1 and LD1, the linear cases, can be very inaccurate even though thin plates are considered. This phenomenon is basically due to the fact that the considered temperature loading possesses a linear z-distribution in the plate. As a consequence, the related transverse normal thermal strains are linear. Such a linear distribution requires at least a quadratic transverse displacement field u_z in each layer that is not considered by LM1 or LD1 analysis (see ω_{zz} vs z diagrams plotted in Figures 7 and 10). Such inaccuracy is much more evident for the ESL-type analyses. Classical Kirchhoff-type analysis (Classical Lamination Theory, CLT),

which neglects any transverse normal strains effect, matches the exact solution of thin plates. This does not happen for the EMZC1, EMC1, EDZ1, or ED1 cases, which, having a linear transverse displacement field u_z, force a constant, nonphysical distribution of transverse strains that causes errors even though thin plates are analyzed. To obtain further insight into this phenomenon, further analyses are provided in Table 4, where the accuracy of the different theories is compared for the two cases of constant and linear $T(z)$. It has been demonstrated that the known performance of LD1 as well as that of ED1 theories has been confirmed for the constant $T(z)$ case for both thin and thick plate geometries. One could conclude that the form of the through-the-thickness distribution of $T(z)$ has an enormous influence on the accuracy of two-dimensional modeling of thermally loaded plates.

CONCLUDING REMARKS

By employing the classical PVD and RMVT, this article presented the differential equations that govern the thermomechanical static behavior of anisotropic multilayered plates modeled using both layer-wise and equivalent single-layer theories. The order N of the expansion used for unknown stress and displacement variables in the layer and/or plate thickness was taken as a free parameter.

A numerical investigation was conducted for the bending of orthotropic, symmetric and unsymmetric cross-ply laminated, simply supported, thick and thin plates for which closed-form solutions are given; the N-values vary from linear to fourth-order expansions.

From a two-dimensional modeling point of view, one can notice that the proposed mixed theory consists of the unique layer-wise analysis, which permits one to *completely* and *a priori* fulfill the C_z^0-continuity conditions at the interfaces for both displacement and transverse stress components (transverse displacement and transverse normal stress included). Nevertheless, the conducted numerical analyses have shown, by means of several comparisons, that the mixed models lead to a better description than the standard displacement models. Furthermore, the related results match the three-dimensional elasticity solutions very well and their accuracy was confirmed for symmetric, unsymmetric, as well as stress and displacement variables of thin and thick multilayered plates. The convenience of referring to RMVT rather than to corresponding theories formulated on the basis of PVD is clearly evident for the ESLM cases.

Future investigations should be addressed to further problems related to different geometries, loadings, boundary conditions, as well as the stacking sequence of multilayered plates. The analysis of the influence of through-the-thickness temperature distributions on the accuracy of the considered plate theories could be of particular interest.

REFERENCES

1. E. A. Thornton, *Thermal Structures for Aerospace Applications*, American Institute of Aeronautics and Astronautics Journal Educational Series, Reston, VA, 1996.
2. S. Srinivas and A. K. Rao, A Note on Flexure of Thick Rectangular Plates and Laminates with Variation of Temperature Across the Thickness, *Bull. Acad. Pol. Sci. Ser. Sci. Tech.*, vol. 20, pp. 229–234, 1972.
3. M. N. Bapu Rao, 3D Analysis of Thermally Loaded Thick Plates, *Nuclear Engrg. and Design*, vol. 55, pp. 353–361, 1979.
4. H. Murakami, Assessment of Plate Theories for Treating the Thermomechanical Response of Layered Plates, *Composite Engrg*, vol. 3, no. 2, pp. 137–149, 1993.
5. V. B. Tungikar and K. M. Rao, Three Dimensional Exact Solution of Thermal Stresses in Rectangular Composite Laminates, *Composite Structures*, vol. 27, pp. 419–427, 1994.
6. K. Bhaskar, T. K. Varadan, and J. S. M. Ali, Thermoelastic Solution for Orthotropic and Anisotropic Composites Laminates, *Composites Pt. B*, vol. 27, pp. 415–420, 1986.
7. E. Carrera, A Class of Two Dimensional Theories for Multilayered Plates Analysis, *Atti Acad. Sci. Torino Mem. Sci. Fis.*, vol. 19–20, pp. 49–87, 1995.
8. T. R. Tauchert, Thermally Induced Flexure, Buckling and Vibration of Plates, *Appl. Mech. Review*, vol. 44, no. 8, pp. 347–360, 1991.
9. A. K. Noor and W. S. Burton, Computational Models for High-temperature Multilayered Composite Plates and Shells, *Appl. Mech. Review*, vol. 45, no. 10, pp. 419–446, 1992.
10. J. Argyris and L. Tenek, Recent Advances in Computational Thermostructural Analysis of Composite Plates and Shells with Strong Nonlinearities, *Appl. Mech. Review*, vol. 50, no. 5, pp. 285–306, 1997.
11. J. N. Reddy, *Mechanics of Laminated Composite Plates, Theory and Analysis*, CRC Press, Boca Raton, FL, 1997.
12. W. H. Pell, *Thermal Deflection of Anisotropic Thin Plates*, vol. 4, no. 1, 1946.
13. Y. Stavsky, Thermoelasticity of Heterogeneous Oleotropic Plates, *J. Engrg. Mech. Division, ASCE*, vol. 89, pp. 89–105, 1963.
14. C. H. Wu and T. R. Tauchert, Thermoelastic Analysis of Laminated Plates 1. Symmetric Specially Orthotropic Laminates, 2. Antisymmetric Angle-Ply and Cross-Ply Laminates, *J. Thermal Stresses*, vol. 3, pp. 247–259, 1980.
15. C. H. Wu and T. R. Tauchert, Thermoelastic Analysis of Laminated Plates 2. Antisymmetric Angle-Ply and Cross-Ply Laminates, *J. Thermal Stresses*, vol. 3, pp. 365–378, 1980.
16. S. A. Ambartsumian, Theory of Anisotropic Plates, Transl. by T. Cheron, J. E. Ashton (Ed.), Technomic, Stamford, CT, 1970.
17. Y. C. Das and B. K. Rath, Thermal Bending of Moderately Thick Rectangular Plates, *Amer. Inst. Aeronautics Astronautics J.*, vol. 10, no. 10, pp. 1349–1351, 1972.
18. V. M. Tolkachev and V. M. Shpektorov, Modification of Reissner Plate Theory for Contact Problems with Temperature Loads, *Soviet Appl. Mech.*, vol. 16, pp. 56–59, 1980.
19. J. M. Whitney, The Effects of Transverse Shear Deformation on the Bending of Laminated Plates, *J. Composite Mats.*, vol. 3, pp. 534–547, 1969.
20. J. N. Reddy, C. W. Bert, Y. S. Hsu, and V. S. Reddy, Thermal Bending of Rectangular Plates of Bimodulus Composite Materials, *J. Mech. Engrg. Sci.*, vol. 22, pp. 297–304, 1980.
21. J. N. Reddy and Y. S. Hsu, Effects of Shear Deformation and Anisotropy on the Thermal Bending of Layered Composite Plates, *J. Thermal Stresses*, vol. 3, pp. 475–493, 1980.
22. L. P. Khoroshun, Method of Constructing Equations of the Shear Theory of Thermoelasticity of Laminate Plates and Shells, *Soviet Appl. Mech.*, vol. 16, no. 10, pp. 851–858, 1981.
23. N. D. Pankratova, A. O. Rasskazov, A. G. Bondar, and A. G. Bondarskii, Thermostress State of Shear-pliable Multilayer Orthotropic Shells and Plates, *Soviet Appl. Mech.*, vol. 23, no. 7, pp. 658–663, 1988.
24. K. N. Cho, C. W. Bert, and A. G. Striz, Thermal Stress Analysis of Laminate Using Higher Order Individual-Layer Theory, *J. Thermal Stresses*, vol. 12, pp. 321–332, 1989.
25. A. A. Kheider and J. N. Reddy, Thermal Stress and Deflections of Cross-ply Laminated Plates Using Refined Theories, *J. Thermal Stresses*, vol. 12, pp. 321–332, 1991.

26. E. Carrera, C_z^0-Requirements: Models for the Two-Dimensional Analysis of Multilayered Structures, *Composite Structures*, vol. 37, pp. 373–384, 1997.
27. E. Carrera, Evaluation of Layer-Wise Mixed Theories for Laminated Plates Analysis, *Amer. Inst. Aeronautics Astronautics J.*, vol. 36, pp. 830–839, 1998.
28. E. Carrera, Mixed Layer-Wise Theories for Multilayered Plates Analysis, *Composite Structures*, vol. 43, pp. 57–70, 1998.
29. E. Carrera, Layer-Wise Mixed Models for Accurate Vibration Analysis of Multilayered Plates, *J. Appl. Mech.*, vol. 65, pp. 820–829, 1998.
30. E. Carrera, A Reissner's Mixed Variational Theorem Applied to Vibrational Analysis of Multilayered Shell, *J. Appl. Mech.*, vol. 66, no. 1, pp. 69–78, 1998.
31. E. Carrera, Multilayered Shell Theories that Account for a Layer-Wise Mixed Description. Part I. Governing Equations, *Amer. Inst. Aeronautics Astronautics J.*, vol. 37, no. 9, pp. 1107–1116, 1999.
32. E. Carrera, Multilayered Shell Theories that Account for a Layer-Wise Mixed Description. Part II. Numerical Evaluations, *Amer. Inst. Aeronautics Astronautics J.*, vol. 37, no. 9, pp. 1117–1124, 1999.
33. E. Carrera, A Study of Transverse Normal Stress Effects on Vibration of Multilayered Plates and Shells, *J. Sound Vibration*, vol. 225, no. 5, pp. 803–828, 1999.
34. E. Carrera, Single-Layer vs Multi-Layers Plate Modelings on the Basis of Reissner's Mixed Theorem, *Amer. Inst. Aeronautics Astronautics J.*, vol. 38, no. 2, pp. 342–352, 2000.
35. E. Reissner, On a Certain Mixed Variational Theory and a Proposed Application, *Int. J. Numer. Methods Engrg.*, vol. 20, pp. 1366–1368, 1984.
36. E. Reissner, On a Mixed Variational Theorem and on a Shear Deformable Plate Theory, *Int. J. Numer. Methods Engrg.*, vol. 23, pp. 193–198, 1986.
37. A. K. Noor and W. S. Burton, Stress and Free Vibration Analyses of Multilayered Composite Plates, *Composite Structures*, vol. 11, pp. 183–204, 1989.
38. R. M. Jones, *Mechanics of Composite Materials*, McGraw-Hill, New York, 1975.
39. H. Murakami, Laminated Composite Plate Theory with Improved In-plane Response, *J. Appl. Mech.*, vol. 53, pp. 661–666, 1986.

APPENDIX

The arrays in the mixed Hooke's law that refer to a generic fiber orientation with respect to the x-axis are

$$\boldsymbol{C}^k_{\mathrm{pp}} = \begin{bmatrix} C^k_{11} & C^k_{12} & C^k_{16} \\ C^k_{12} & C^k_{22} & C^k_{26} \\ C^k_{16} & C^k_{26} & C^k_{66} \end{bmatrix} \qquad \boldsymbol{C}^k_{\mathrm{pn}} = \begin{bmatrix} 0 & 0 & C^k_{13} \\ 0 & 0 & C^k_{23} \\ 0 & 0 & C^k_{36} \end{bmatrix}$$

$$\boldsymbol{C}^k_{\mathrm{np}} = \begin{bmatrix} 0 & 0 & 0 \\ 0 & 0 & 0 \\ -C^k_{13} & -C^k_{23} & -C^k_{36} \end{bmatrix} \qquad \boldsymbol{C}^k_{\mathrm{nn}} = \begin{bmatrix} C^k_{55} & -C^k_{45} & 0 \\ -C^k_{45} & C^k_{44} & 0 \\ 0 & 0 & C^k_{33} \end{bmatrix}$$

where

$$C^k_{ij} = \tilde{C}^k_{ij} - \frac{\tilde{C}^k_{i3}\tilde{C}^k_{3j}}{\tilde{C}^k_{33}} \quad i,j = 1,2,6 \qquad C^k_{i3} = \frac{\tilde{C}^k_{i3}}{\tilde{C}^k_{33}} \quad i = 1,2,6$$

$$C^k_{33} = \frac{1}{\tilde{C}^k_{33}} \qquad C^k_{44} = \frac{\tilde{C}^k_{44}}{\Delta} \qquad C^k_{55} = \frac{\tilde{C}^k_{55}}{\Delta} \qquad C^k_{45} = \frac{\tilde{C}^k_{45}}{\Delta} \qquad \Delta = \tilde{C}^k_{44}\tilde{C}^k_{55} - (C^k_{45})^2$$

The arrays of differential operators on Ω^k are

$$\boldsymbol{D}_{\mathrm{p}} = \begin{bmatrix} \partial_x & 0 & 0 \\ 0 & \partial_y & 0 \\ \partial_y & \partial_x & 0 \end{bmatrix} \qquad \boldsymbol{D}_{\mathrm{n}} = \begin{bmatrix} \partial_z & 0 & \partial_x \\ 0 & \partial_z & \partial_y \\ 0 & 0 & \partial_z \end{bmatrix}$$

$$\boldsymbol{D}_{\mathrm{n}\Omega} = \begin{bmatrix} 0 & 0 & \partial_x \\ 0 & 0 & \partial_y \\ 0 & 0 & 0 \end{bmatrix} \qquad \boldsymbol{D}_{\mathrm{n}z} = \begin{bmatrix} \partial_z & 0 & 0 \\ 0 & \partial_z & 0 \\ 0 & 0 & \partial_z \end{bmatrix}$$

The additional arrays introduced in Eq. (29) are

$$\boldsymbol{I} = \begin{bmatrix} 1 & 0 & 0 \\ 0 & 1 & 0 \\ 0 & 0 & 1 \end{bmatrix} \qquad \boldsymbol{I}_{\mathrm{p}} = \begin{bmatrix} 1 & 0 & 0 \\ 0 & 1 & 0 \\ 1 & 1 & 0 \end{bmatrix} \qquad \boldsymbol{I}_{\mathrm{n}\Omega} = \begin{bmatrix} 0 & 0 & 1 \\ 0 & 0 & 1 \\ 0 & 0 & 0 \end{bmatrix}$$